Decadal Relationship between European Blocking and the North Atlantic Oscillation during 1978–2011. Part I: Atlantic Conditions

DEHAI LUO

RCE-TEA, Institute of Atmospheric Physics, Chinese Academy of Science, Beijing, Qingdao Collaborative Innovation Center of Marine Science and Technology, Qingdao, China

YAO YAO

RCE-TEA, Institute of Atmospheric Physics, Chinese Academy of Science, Beijing, and Physical Oceanography Laboratory, College of Physical and Environmental Oceanography, Ocean University of China, Qingdao, China

AIGUO DAI

Department of Atmospheric and Environmental Sciences, University at Albany, State University of New York, Albany, New York, and National Center for Atmospheric Research, Boulder, Colorado

(Manuscript received 6 March 2014, in final form 15 November 2014)

ABSTRACT

Both the positive and negative phases of the North Atlantic Oscillation (NAO^+ and NAO^-, respectively) and atmospheric blocking in the Euro-Atlantic sector reflect synoptic variability over the region and thus are intrinsically linked. This study examines their relationship from a decadal change perspective. Since the winter-mean NAO index is defined as a time average of instantaneous NAO indices over the whole winter, it is unclear how the activity of European blocking (EB) events can be related to the variation of the positive mean NAO index. Here, this question is examined by dividing the winter period 1978–2011 into two decadal epochs: 1978–94 (P1) with an increasing and high NAO index and 1995–2011 (P2) with a decreasing and low NAO index. Using atmospheric reanalysis data, it is shown that there are more intense and persistent EB events in eastern Europe during P1 than during P2, while the opposite is true for western Europe.

It is further shown that there are more NAO^+ (NAO^-) events during P1 (P2). The EB events associated with NAO^+ events extend more eastward and are associated with stronger Atlantic mean zonal wind and weaker western Atlantic storm track during P1 than during P2, but EB events associated with NAO^- events increase in western Europe under opposite Atlantic conditions during P2. Thus, the increase in the number of individual NAO^+ (NAO^-) events results in more EB events in eastern (western) Europe during P1 (P2). The EB change is also associated with the increased frequency of NAO^- to NAO^+ (NAO^+ to NAO^-) transition events.

1. Introduction

In recent years, extreme cold events in winter have occurred frequently in Europe (Zhang et al. 2012). They caused persistent cold outbreaks and anomalous snowfalls in the Euro-Atlantic and its adjacent regions (Sillmann and Croci-Maspoli 2009; Sillmann et al. 2011). The extreme cold European winters were found to be related to not only the negative phase of the North Atlantic Oscillation (NAO) (Yiou and Nogaj 2004; Scaife et al. 2008; Cattiaux et al. 2010; Seager et al. 2010; Sillmann et al. 2011), but also to atmospheric blocking in the Euro-Atlantic sector (Tyrlis and Hoskins 2008a,b; Buehler et al. 2011; Sillmann et al. 2011). By definition, the NAO index and atmospheric blocking in the Euro-Atlantic sector are related, and they both reflect changes in atmospheric pressure fields associated with synoptic variability in the region. Thus, it is no surprise that there is an anticorrelation between the NAO and blocking events over the Atlantic region (Shabbar et al. 2001; Scherrer et al. 2006), as well as a positive correlation between the

Corresponding author address: Dr. Dehai Luo, RCE-TEA, Institute of Atmospheric Physics, Chinese Academy of Science, Beijing 100029, China.
E-mail: ldh@mail.iap.ac.cn

DOI: 10.1175/JAS-D-14-0039.1

NAO and blocking events over Europe (Croci-Maspoli et al. 2007a). In particular, during winters with a positive NAO phase (NAO^+), significantly intensified (reduced) blocking frequency is found in Europe (the North Atlantic), and vice versa for the negative NAO phase (NAO^-) (Luo et al. 2007a; Woollings et al. 2008). The longitudinal position of Euro-Atlantic blocking events in winter is important for whether the winter cold events over the European continent are severe, as suggested by Sillmann et al. (2011). Thus, investigating the dynamical cause of the variability of blocking events in the Euro-Atlantic sector can improve our understanding of the genesis of recent winter extreme cold events over Europe.

Many studies have examined the relationship between the phase of NAO events and blocking events over Greenland, the North Atlantic, and Europe (Shabbar et al. 2001; Croci-Maspoli et al. 2007a; Woollings et al. 2008; Davini et al. 2012a). Some studies also suggested that NAO^- events arise mostly from the retrogression (i.e., westward migration) of European blocking (EB) events through the amplification of blocking ridges over northern Europe under the synoptic eddy forcing in the Atlantic storm track (Feldstein 2003; Woollings and Hoskins 2008; Sung et al. 2011).

It is well known that the winter-mean NAO index, defined as a time average of all daily indices in winter, including those of NAO^+, NAO^-, and regime transition events in winter, exhibits clear interdecadal variability from a dominant negative-phase epoch (1950–77) to a dominant positive-phase epoch (1978–2011) (Hurrell 1995; https://climatedataguide.ucar.edu/climate-data/hurrell-north-atlantic-oscillation-nao-index-pc-based). The decadal relationship between the winter-mean NAO index and the Euro-Atlantic blocking frequency from the 1960s to the 1990s has been investigated by many researchers (Shabbar et al. 2001; Croci-Maspoli et al. 2007a; Davini et al. 2012a). For example, Shabbar et al. (2001) examined the correlation between the Euro-Atlantic blocking and the decadal variation of the winter-mean NAO index from 1960–70 (dominant negative phase) to 1980–90 (dominant positive phase). They found that the blocking frequency is enhanced (reduced) in the European continent during 1980–90 (1960–70), and the Atlantic blocking is more persistent during the negative phase of NAO. An EOF analysis by Croci-Maspoli et al. (2007a) shows that long-lasting blocking events in the Atlantic basin are associated with the development of negative-phase NAO events. Woollings et al. (2008) noted that negative (positive)-phase NAO events correspond to the presence of blocked (unblocked) flows or the presence (absence) of cyclonic wave breaking events over the North Atlantic. More recently, Davini et al. (2012a) found that the eastward shift of the NAO pattern during the 1980s and 1990s is associated with an absence of the Greenland blocking.

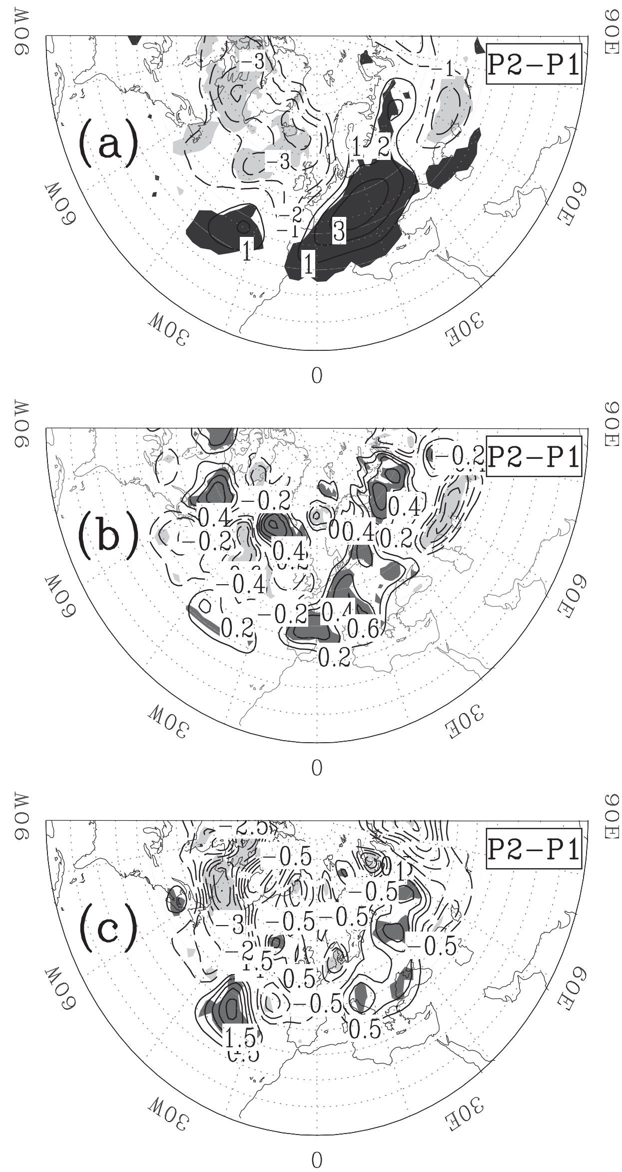

FIG. 1. The P2 − P1 difference of the blocking (a) frequency (%), (b) intensity, and (c) duration between two epochs: P1 (1960–70) and P2 (1980–90), based on the blocking index of Davini et al. (2012b). The gray denotes the regions above the 95% confidence level for a two-sided Student's t test.

The decadal variation of the Euro-Atlantic blocking from a dominant negative winter-mean NAO index during 1960–70 to a dominant positive winter-mean NAO index during 1980–90 can be seen from Fig. 1 based on the blocking index of Davini et al. (2012a), as described below. It is clear that the EB events are more frequent as the winter-mean NAO index is in a dominant positive phase during 1980–90, when the blocking is more intense but less persistent over Greenland and the

North Atlantic. In contrast, the EB events are less frequent during 1960–70.

Although some of these interdecadal changes have been noted by Shabbar et al. (2001), Croci-Maspoli et al. (2007a), and Davini et al. (2012a), it is unclear whether the change of the winter-mean NAO index with dominant NAO^+ events in the recent three decades (1978–2011) can lead to (or is associated with) a marked decadal change in EB events. This question arises because the winter-mean NAO index exhibits an upward trend from 1978–94 and a weak downward trend after 1994 (Cohen and Barlow 2005). In this paper, we attempt to address two outstanding questions: 1) Can the EB events, in their frequency, position, intensity, and duration, exhibit a significant decadal variation as the positive winter-mean NAO index undergoes a change around 1994? 2) What factors determine the decadal variation of the winter EB events if there is such a change?

In our previous studies (Luo et al. 2011, 2012a,b), we examined under what conditions the NAO regime transition events occur and how the regime transition leads to the variation of the winter-mean NAO index and found that the frequency change in NAO regime transition events is important for the interannual variability of the winter-mean NAO index. However, these studies did not answer the questions proposed above. The aim of the present paper is to reveal the relationship between EB events (i.e., intensity, duration, and position) and the long-term variations of the winter-mean NAO index during 1978–2011 and the different roles of individual NAO and regime transition events associated with Atlantic background conditions in the EB variability. In this study, we present new findings that more intense and persistent blocking events tend to occur in eastern (western) Europe during 1978–94 (1995–2011), associated with the intensification (weakening) of the Atlantic mean zonal wind and or the weaker (stronger) Atlantic storm track as the positive winter-mean NAO index exhibits an increasing (a decreasing) trend. The causality or the dynamics of the decadal variations of the EB events is investigated in Luo et al. (2015, hereafter Part II).

To address the above questions, we divide 1978–2011 into two decadal epochs: an increasing and high (1978–94; P1) and a decreasing and low (1995–2011; P2) NAO index period. By examining the difference of the Euro-Atlantic blocking events between P1 and P2 using a bidimensional blocking index, we can quantify the decadal changes in the EB events. Furthermore, we investigate which types of the NAO events contribute more (or are more closely related) to the variation of the EB events from P1 to P2 by calculating the frequencies of individual NAO events and regime transition events during P1 and P2, as well as the associated blocking frequency difference. The different Atlantic background conditions, which affect the decadal variations of the EB events from P1 to P2, are also examined using the difference of the winter-mean zonal wind and eddy kinetic energy (EKE) between P1 and P2 (with the NAO events excluded). The results can improve our understanding of the decadal shifts in EB events.

This paper is organized as follows. Section 2 describes data and the detection method for blocking events. In section 3, we present results on the location, intensity, and duration of the EB events during epoch P1 and P2. We examine the different contributions of different types of NAO events to the decadal variations of EB events in section 4. The relationship between the two NAO phases and the EB events are investigated in section 5. In section 6, we examined the relationship between the blocking position of the EB events and the Atlantic mean zonal wind and western Atlantic storm-track strengths. Conclusions and discussions are summarized in section 7. In Part II, the dynamical mechanism through which the Atlantic conditions affect the EB activity will be investigated using a nonlinear multiscale interaction model.

2. Data and detection method for blocking events

a. Data

We used the 2.5° daily data of primarily 500-hPa geopotential height from the National Centers for Environmental Prediction–National Center for Atmospheric Research (NCEP–NCAR) reanalysis (Kalnay et al. 1996) from 1978–2011, during which most of the winters have positive mean NAO index values. Moreover, the ERA-Interim data from 1979 to 2011 were also used to evaluate the sensitivity of our results to different datasets. The winter is defined here as November–March (NDJFM). In the following calculations, 1978/79–2011/12 is referred to as 1978–2011. When the period 1978/79–2011/12 is split into two epochs: 1978/79–94/95 and 1995/96–2011/12, the two epochs are defined as 1978–94 and 1995–2011, respectively. The other splitting of a period has the same definition.

The daily (monthly) NAO index, defined as the time series of the leading rotated empirical orthogonal function (REOF1) of daily (monthly) geopotential height fields at 500 hPa in the Northern Hemisphere (NH), was obtained from the NOAA Climate Prediction Center (CPC) (ftp://ftp.cpc.ncep.noaa.gov/cwlinks/). The winter-mean NAO index used here is slightly different from Hurrell's NAO index (Hurrell 1995). We used a time mean of daily NAO indices during a 5-month period from November to March, instead of the 4-month time-mean winter NAO index from December to March (DJFM) in the Hurrell's NAO index. Our calculation indicated that the difference of the results between the two NAO indices is very small (not shown). Here, we only show the winter (NDJFM)-mean NAO index (Fig. 2). In summary, we used the daily NAO index to define the individual NAO and transition events (as defined below) and their occurrence frequency during each winter and also averaged the daily NAO index to derive the winter-mean NAO index and the composite daily NAO index averaged over different types of the NAO events.

In previous studies (Lejenäs and Økland 1983; Tibaldi and Molteni 1990; Pelly and Hoskins 2003; Diao et al. 2006; Scherrer et al. 2006; Barriopedro et al. 2006, 2010; Croci-Maspoli et al. 2007b; Davini et al. 2012a,b), many one-dimensional (1D) and two-dimensional (2D) blocking indices have been used to quantify the NH blocking activity. Croci-Maspoli et al. (2007b) and Barriopedro et al. (2010) constructed 2D blocking indices based upon the vertically averaged potential vorticity (VAPV) and geopotential height anomalies, respectively. For the VAPV index of Croci-Maspoli et al. (2007b), in the Euro-Atlantic sector the maximum winter blocking frequency is over the Atlantic basin, rather than over the European continent (their Fig. 2a). However, as shown by the blocking indices of Tibaldi and Molteni (1990), Diao et al. (2006), and Davini et al. (2012b), the maximum frequency of Euro-Atlantic blocking events is over the European continent, rather than the Atlantic basin. The analysis from the blocking index of Barriopedro et al. (2010) further shows that the maximum frequency of winter blocking is located over the European continent, rather than over the Atlantic basin (their Fig. 4a), consistent with the results of Diao et al. (2006, their 6a), although the index definitions are slightly different. In essence, the 2D blocking index of Barriopedro et al. (2010) is similar to that of Diao et al. (2006), who used the total height field in contrast to the anomaly height field used by Barriopedro et al. (2010). This is because the difference of the result between these two indices based on the anomaly and absolute fields is small because the blocking flow is usually weak in a climatological field. This difference can also be seen from the comparison between the results of Diao et al. (2006, their Figs. 6a and 11a) and Barriopedro et al. (2010, their Figs. 4a and 8a). Thus, it is reasonable to use the 2D index of Diao et al. (2006) to diagnose the blocking activity in the Euro-Atlantic sector. On the other hand, because the 2D index of Davini et al. (2012b) can differentiate high- and mid-latitude (Greenland and European Continent) blockings, here we use the two 2D blocking indices of Diao et al. (2006) and Davini et al. (2012b) to depict the blocking activity in winter in the Euro-Atlantic sector during 1978–2011 and compare the results. The first index we use is the 2D blocking index by Davini et al. (2012b) (DCGN index), which is defined based on the strength of the meridional gradient of the 500-hPa geopotential height. The second one is the 2D blocking index proposed by Diao et al. (2006) (DLL index), which is defined based on the difference of the 500-hPa geopotential height at a given latitude and the reference latitude to its southern side. In the DLL index, the reference latitude is selected as the latitude position of the minimum value of the composite height of the blocking events (Diao et al. 2006).

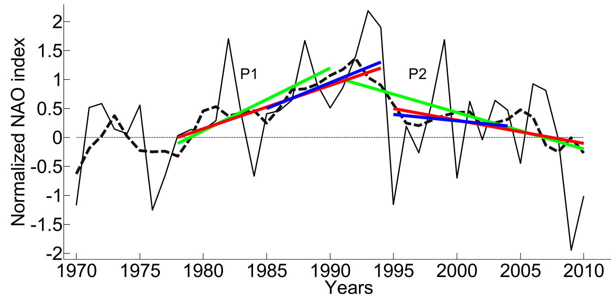

FIG. 2. Time series (solid line) of the normalized winter-mean NAO index obtained by averaging the monthly NAO index at 500 hPa [obtained from the CPC (http://www.cpc.noaa.gov/)] for NDJFM from 1970 to 2011. The red lines denote the linear upward and downward trends during P1 (1978–94) and P2 (1995–2011). The green lines denote the case of P1 (1978–90) and P2 (1991–2011). The blue lines represent the case of P1 (1985–94) and P2 (1995–2004). The dashed line is a five-point moving average.

For the DCGN index, low-latitude blocking events in the Atlantic basin are significantly overestimated, because the long-lasting high pressure systems over the eastern Atlantic, often defined as strong persistent ridge events (SPREs) by Santos et al. (2009), are included in this index. In addition, the DCGN index seems to overestimate the frequency of high-latitude blocking events in the Pacific basin compared to other previous indices (Tibaldi and Molteni 1990). For the DLL index, high-latitude blocking events over Greenland are underestimated, while the overestimation of low-latitude blocking events is avoided. To examine whether our results are sensitive to the choice of the blocking index, we use both the DCGN and DLL indices, with the DCGN index used in most of the results presented here.

In this study, the lag-and-lead relationship between individual NAO and blocking events are also examined using their daily indices over the life cycle of an NAO event, with the time axis being the number of days before (negative lag) and after (positive lag) the day when the NAO event peaks.

b. DCGN index

The DCGN index is a 2D extension of the blocking index proposed by Tibaldi and Molteni (1990). The basic idea of this index is similar to that of the 2D blocking index of Scherrer et al. (2006). The DCGN index is defined as the meridional gradients of daily 500-hPa geopotential height at each longitude:

$$\mathrm{GHGS}(\lambda,\phi) = \frac{Z(\lambda,\phi) - Z(\lambda,\phi_S)}{\phi - \phi_S}, \qquad (1a)$$

$$\mathrm{GHGN}(\lambda,\phi) = \frac{Z(\lambda,\phi_N) - Z(\lambda,\phi)}{\phi_N - \phi}, \qquad (1b)$$

where λ (ϕ) is the longitude (latitude) at a given grid point, $\phi_N = \phi + 15°$, $\phi_S = \phi - 15°$; λ (ϕ) ranges in longitudes from 0° to 360° (latitudes 30°–75°N); and $Z(\lambda, \phi)$ is the daily 500-hPa geopotential height at the grid point (λ, ϕ). Note that GHGN and GHGS represent the meridional gradients of geopotential height at the northern and southern sides of a given grid point (λ, ϕ), respectively. An instantaneous blocking (IB) is identified if the constraint condition in (1c) is satisfied:

$$\begin{aligned}&\mathrm{GHGS}(\lambda,\phi) > 0,\\ &\mathrm{GHGN}(\lambda,\phi) < -10\,\mathrm{m\ per\ }1°\mathrm{\ of\ latitude},\end{aligned} \qquad (1c)$$

$$\mathrm{GHGS}_2(\lambda,\phi) = \frac{Z(\lambda,\phi_S) - Z(\lambda,\phi_S - 15°)}{15°} < -5\,\mathrm{m\ per\ }1°\mathrm{\ of\ latitude}. \qquad (1d)$$

In this paper, because our focus is placed on relatively high-latitude blocking events, low-latitude blocking events and subtropical ridges in the Euro-Atlantic sector are excluded by adding the constraint in (1d) to the blocking index defined in (1a) and (1b).

Here, a large-scale blocking event is defined at grid point (λ, ϕ) if the instantaneous blocking event is occurring within a box of 10° longitude by 5° latitude around that grid point for at least 5 days (Davini et al. 2012b). Such criteria ensure that the detected episodes have both significant meridional and zonal extensions and are quasi stationary and persist for sufficient time to be considered as real blocking events. For this case, the ending of a blocking event at a given grid point is implicated if (1c) is not satisfied during the blocking decay. Thus, the duration of a blocking event for each grid point can be estimated by calculating the time interval between the beginning and ending of the required constraint of (1c). The climatological spatial distribution of the blocking duration is obtained by performing the composite average of the blocking duration fields for all blocking events.

Correspondingly, the blocking frequency at a given grid point is defined as the percentage of the persistence days of an IB event divided by the total number of days for the winter. Then, we average the winter blocking frequency from 1978 to 2011 to obtain the climatological blocking frequency distribution.

The blocking intensity is defined as follows (Wiedenmann et al. 2002; Davini et al. 2012a,b):

$$B_I(\lambda,\phi) = 100\left[\frac{Z(\lambda,\phi)}{\mathrm{RC}(\lambda,\phi)} - 1.0\right], \qquad (2a)$$

where

$$\mathrm{RC}(\lambda,\phi) = \frac{[Z_U + Z(\lambda,\phi)]/2 + [Z_D + Z(\lambda,\phi)]/2}{2}, \qquad (2b)$$

Z_U and Z_D are the minimum of the $Z(\lambda, \phi)$ field within 60° upstream and downstream at the same latitude ϕ of the chosen grid point, respectively (Wiedenmann et al. 2002), and RC is a reference geopotential height for the blocking event. Here, a stronger blocking event is detected if B_I has a higher value. Thus, the nondimensional strength of a blocking event can be estimated by calculating the value of B_I.

The climatological distribution of the blocking intensity (BI) is calculated as follows: We first calculate the BI of a blocking event at each grid point for each time step and then make a time average over the entire duration of a blocking event at each grid point to obtain the time-mean BI distribution of a blocking event; second, we average the BI over all winter blocking events for all years to obtain the climatological maps of the BI.

c. DLL index

As described in Diao et al. (2006), the daily DLL blocking index is defined as

$$\mathrm{BI}_j(\lambda,\varphi,t) = \begin{cases} Z(\lambda,\varphi_{rj},t) - Z(\lambda,\varphi,t), & \text{if} \quad Z(\lambda,\varphi,t) > Z(\lambda,\varphi_{rj},t) \quad \text{and} \quad \varphi > \varphi_{rj} \\ 0, & \text{otherwise}, \end{cases} \qquad (3a)$$

$$\mathrm{BI}(\lambda,\varphi,t) = \min_{j=1,2,3}[\mathrm{BI}_j(\lambda,\varphi,t)], \qquad (3b)$$

where t denotes the time (days) and $Z(\lambda, \varphi, t)$ is the daily 500-hPa geopotential height for the gridpoint (λ, φ) that satisfies $360° \geq \lambda \geq 0$ and $90°\mathrm{N} \geq \varphi \geq \varphi_{rj}$, where φ_{rj} can be three chosen reference latitudes at a given longitude. The details of the φ_{rj} choices can be found in Diao et al. (2006).

An instantaneous blocking event can be detected by tracking the area with negative $\mathrm{BI}(\lambda, \varphi, t)$ values from (3) because the blocking flow is reflected by the area with negative $\mathrm{BI}(\lambda, \varphi, t)$ values. To a large extent, the blocking region contains many isolated negative $\mathrm{BI}(\lambda, \varphi, t)$ areas because the blocking region is often comprised of several isolated anticyclones and cyclones (Berggren et al. 1949). In this case, the amplitude of the negative $\mathrm{BI}(\lambda, \varphi, t)$ for each isolated area within the blocking region is defined as

$$M_i'(t) = \max_{\lambda,\varphi\in\Omega_i} |\mathrm{BI}(\lambda,\varphi,t)|, \quad i = 1,2,\ldots,n, \qquad (4)$$

where Ω_i is the area of each isolated area, and n is the number of the isolated negative $\mathrm{BI}(\lambda, \varphi, t)$ area.

The instantaneous amplitude $M'(t)$ of a blocking event on each day is defined as the strongest one of $M_i'(t)$:

$$M'(t) = \max[M_i'(t)], \quad i = 1,2,\ldots,n. \qquad (5)$$

The day when there is the negative $\mathrm{BI}(\lambda, \varphi, t)$ area and when $M'(t) \geq 50$ $[M'(t) \leq 50]$ gpm is satisfied simultaneously is defined as the onset (termination) day of a blocking event. Correspondingly, the number of days of a persistent negative $\mathrm{BI}(\lambda, \varphi, t)$ process between the onset and termination of an event is defined as the duration of the blocking. If the duration is equal to 5 days or longer, then this event is considered a blocking event. Different from the definition of Diao et al. (2006), here the intensity of a blocking event is defined as a time average of $M'(t)$ from the onset of a blocking event to its termination, which is also different from the definition of the blocking intensity in the DCGN index.

d. *Division of the 1978–2011 period in winter*

To examine how the variation of the positive winter-mean NAO index in the recent three decades affects the long-term variation of EB events, it is reasonable to split the period from 1978 to 2011 into two epochs, because of the positive winter-mean NAO index undergoing a substantial decadal change around the 1990s. In addition, to further test the sensitivity of our results to the two different epochs of 1978–2011, we consider three cases. The first case is to split 1978–2011 into 1978–94 (P1) and 1995–2011 (P2), because the trend reversal of the winter-mean NAO index is after 1994. The second case is to divide 1978–2011 into 1978–90 (P1) and 1991–2011 (P2) based on the studies of Cohen and Barlow (2005) and Luo et al. (2012a,b). The third case is to assume that P1 (P2) corresponds to 1985–94 (1995–2004), because the NAO index was very positive in 1985–94. In this paper, the variation of EB or NAO events from P1 to P2 is simply referred to as a "decadal" shift or variation. Such a decadal variation definition is different from the previous definitions of the decadal variations of blocking events investigated by Chen and Yoon (2002) and Croci-Maspoli et al. (2007b) and NAO events studied by Shabbar et al. (2001) and Wang and Magnusdottir (2012) from 1958–77 to 1978–97.

3. Recent decadal shifts in European blocking

a. *Decadal shifts of blocking location, intensity, and duration over Europe*

Here, we first use the DCGN index to calculate the IB frequency to reflect the geographical distribution of EB events, because the spatial distribution of the IB frequency is almost identical to that of the blocking event frequency (Davini et al. 2012a,b). Then we show the long-term climatology of the blocking frequency (Fig. 3) over the Euro-Atlantic sector based on two types of reanalysis data and compare their difference to strengthen our conclusion. The P2 − P1 difference fields of the blocking intensity and duration are shown in Fig. 4. It is seen (Figs. 3a–c) that for the NCEP–NCAR reanalysis data, the IB frequency has two distinct maxima over Greenland and Europe for P1 (1978–94) and P2 (1995–2011), but the center of action in Europe is shifted southwestward from P1 to P2. This shift is likely related to the southwestward shift of the Atlantic jet stream due to the increased frequency of NAO^- events during P2 (Woollings et al. 2010a). It is also obvious that the blocking frequency over Greenland is increased from P1 to P2. Because the Greenland blocking events are strongly anticorrelated with the NAO index (Woollings et al. 2008), the enhanced Greenland blocking during P2 is tightly related to the increased frequency of NAO^- events (i.e., weaker Icelandic lows) during P2 (Davini et al. 2012a).

The EB events show an enhanced frequency in eastern Europe during P1 as well, as in western Europe during P2. Their frequency difference between P2 and P1 is statistically significant at the 95% confidence level for a two-sided Student's t test (Livezey and Chen 1983). The Student's t test is applicable to even non-Gaussian variables for relatively large samples (>30; Von Storch and Zwiers 2001). Thus, this raises an important result: the blocking frequency is enhanced in eastern Europe

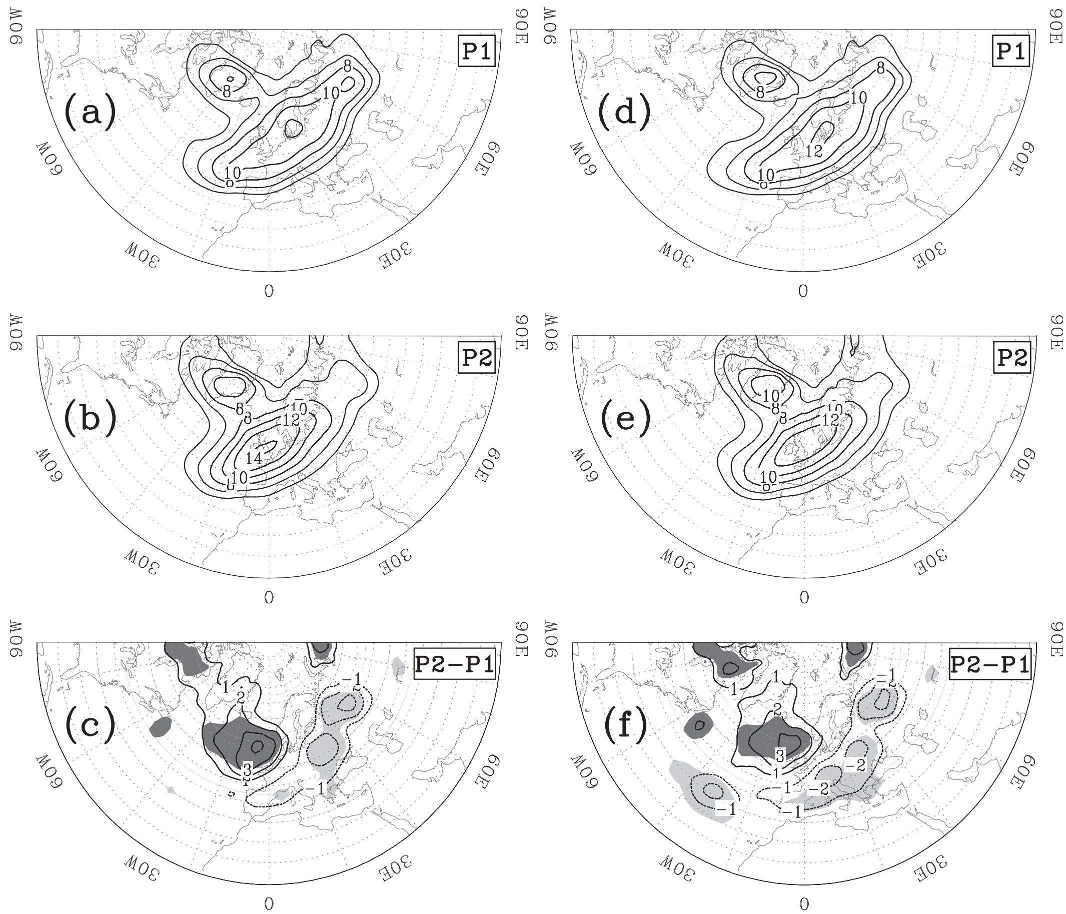

FIG. 3. Horizontal distributions of the winter-mean blocking frequency (%) during the periods (a),(d) P1 (1978–94) and (b),(e) P2 (1995–2011) and (c),(f) the P2 − P1 difference based on the blocking index of Davini et al. (2012b) calculated using the (left) NCEP–NCAR reanalysis and (right) ERA-Interim data. The blocking frequency is defined as the number of days with blocking expressed as a percentage of total number of days for the winter (November–March). The dark (positive) and light (negative) shadings denote the regions above the 95% confidence level for a two-sided Student's *t* test.

(EE, 20°–70°E) during P1 and in western Europe (WE, 20°W–20°E) during P2. A region with small negative values of the P2 − P1 blocking frequency difference in the southern side of WE reflects the contributions from the positive height anomalies associated with NAO^+ events that are stronger during P1 than during P2 (Fig. 2).

It is obvious that more intense EB events tend to occur in EE during P1 and in WE during P2 (Figs. 4a,c). Moreover, the mean blocking duration is longer in EE during P1 and in WE during P2 than in the other period (Figs. 4b,d). Thus, there is an enhanced frequency of more intense and persistent blocking events in EE during P1 and in WE during P2, although there is an evident difference of the epoch difference (P2 − P1) fields for the blocking intensity and duration between the two reanalysis datasets. The results suggest that there are decadal variations of EB events in location, intensity, and duration associated with the decadal change in the winter-mean NAO index seen in Fig. 2. Specifically, when the winter-mean NAO index increases to a high level in P1, the frequency of more intense and persistent EB events exhibits an eastward shift compared with that in P2, when the NAO index is at lower levels.

b. A comparison with the results from ERA-Interim

It is also clear from Figs. 3 and 4 that the results from ERA-Interim are broadly consistent with those from the NCEP–NCAR reanalysis. Thus, our results are insensitive to different reanalysis data, although the reanalyses used similar observations that may contain common errors [e.g., a spurious cooling center over central Asia in both ERA-40 and NCEP–NCAR reanalysis data (Dai et al.

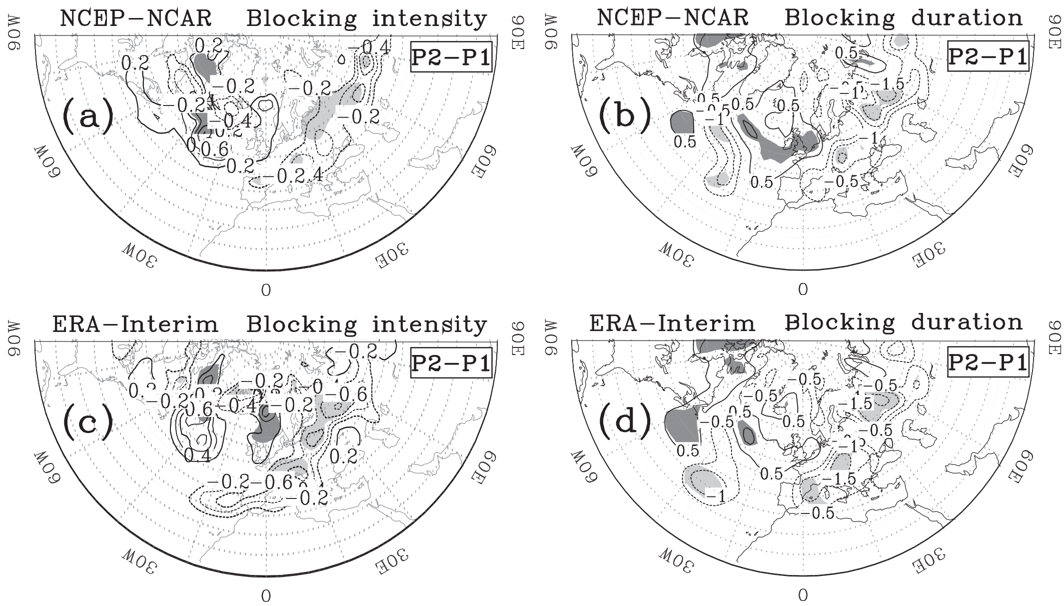

FIG. 4. Epoch (P2 − P1) difference of winter-mean blocking (a),(c) intensity and (b),(d) duration based on the blocking index of Davini et al. (2012b) for P1 (1978–94) and P2 (1995–2011), using the (a),(b) NCEP–NCAR reanalysis and (c),(d) ERA-Interim data. The dark (positive) and light (negative) shadings denote the regions above the 95% confidence level for a two-sided Student's *t* test.

2013)]. Although Davini et al. (2012b) had recently made a comparison of the climatological blocking frequency, intensity, and duration between the two reanalysis datasets, for our study here, such a data comparison is still needed to validate our results. In the following discussions, our focus is placed on the results from the NCEP–NCAR reanalysis data.

c. Impact of different epochs on results

To examine if the above results are very sensitive to different epochs for 1978–2011, we repeated all the calculations for two more cases of different epochs: (i) P1 (1978–90) and P2 (1991–2011) and (ii) P1 (1985–94) and P2 (1995–2004) using the same blocking index and reanalysis data. Figure 5 shows the P2 − P1 difference of the blocking frequency, intensity and duration for these two cases. More intense and persistent EB events are still seen in EE during P1 (1978–90) than during P2 (1991–2011). However, we further see a slightly increased frequency of more intense and persistent blocking events over Greenland during P1 (Figs. 5a–c). A possible cause is that NAO^+ events are fewer during 1978–90 than during 1978–94 (Tables 1 and 2). Such a phenomenon is almost invisible if we use P1 (1985–94) and P2 (1995–2004). This is because epoch 1985–94 has more frequent NAO^+ events (Table 3), thus leading to the absence of blocking over Greenland (Woollings et al. 2008; Davini et al. 2012a). We can see from Figs. 5d–f that there are more frequent, intense, and persistent EB events in EE and in the southern side (lower latitudes) of WE during P1 (1985–94) than during P2 (1995–2004). For P1 (1985–94), a marked increase in the EB frequency over the southern side of WE is more likely to be due to higher NAO^+ event frequency, as noted below. A comparison among Figs. 3–5 also shows that during P2 (1995–2004) the enhanced blocking frequency is shifted westward compared with P1 (1978–94) and located over Greenland, the North Atlantic, and northwestern Europe (Figs. 5d–f) because of an increased frequency of NAO^- events during 1995–2004 (Table 3). Thus, the EB events can exhibit a significant westward displacement as the winter-mean NAO index decreases to a neutral value. As shown below, the westward shift of the blocking frequency is related to the weakening of the Atlantic mean zonal wind associated with the decreased NAO index.

d. A comparison with the DCGN index

To test the sensitivity of our results to different choices of the blocking index, we performed the same calculation as in Figs. 3 and 4 using the DLL index. The differences of the blocking frequency, intensity, and duration between P1 (1978–94) and P2 (1995–2011) shows an enhanced frequency of more intense and persistent EB events in EE during P1 and in WE during P2

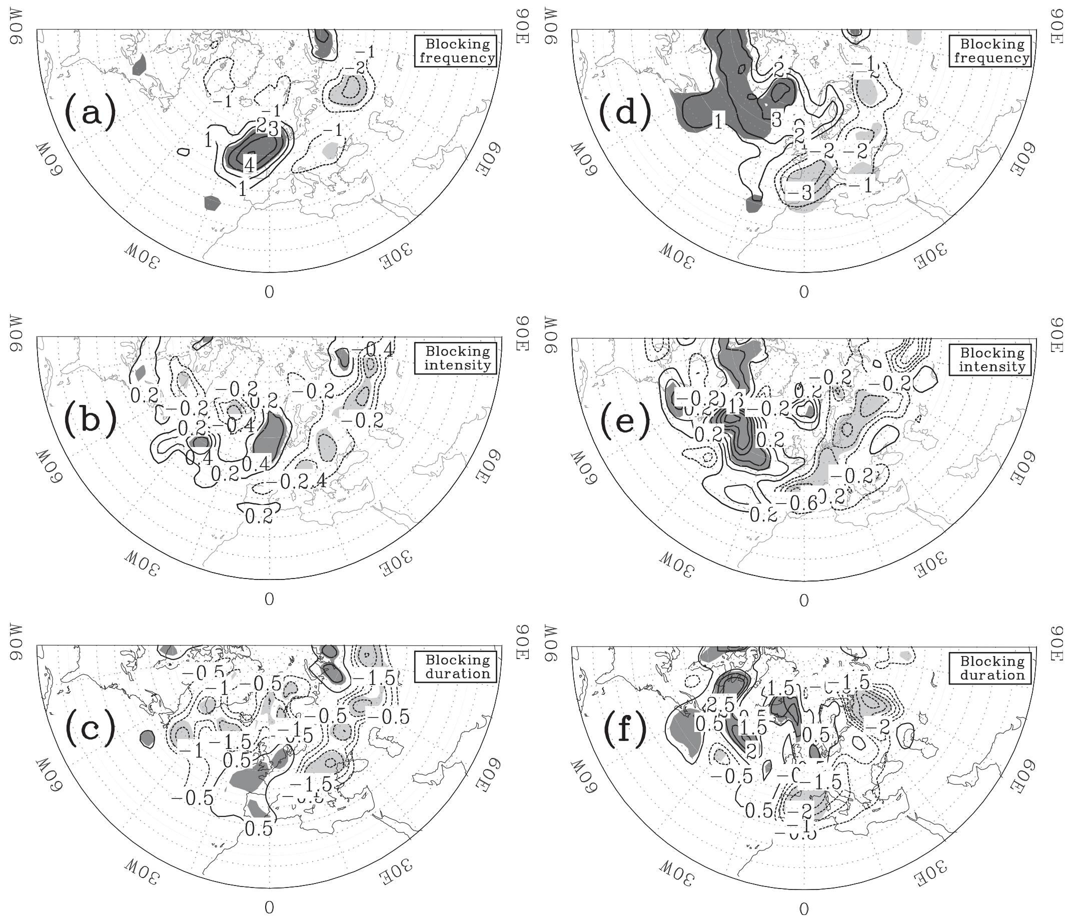

FIG. 5. Epoch (P2 − P1) difference of winter-mean blocking (a),(d) frequency (%); (b),(e) intensity; and (c),(f) duration based on the blocking index of Davini et al. (2012b) for two other definitions of the P1 and P2: (left) P1 (1978–90) and P2 (1991–2011) and (right) P1 (1985–94) and P2 (1995–2004). The dark (positive) and light (negative) shadings denote the region above the 95% confidence level for a two-sided Student's *t* test.

(Fig. 6). This supports our findings from the DCGN index that our main results are insensitive to the choice of the blocking index, although the DLL index cannot sufficiently identify blocking events over Greenland. We notice that Barnes et al. (2012) made a comparison among different indices and found that the duration of blocking events is almost independent of the blocking detection index.

TABLE 1. Number of individual NAO events and NAO transition events in winter during P1 and P2 for case 1: P1 is 1978/79–94/95 and P2 is 1995/96–2011/12.

	Epoch	
	P1 = 17 yr	P2 = 17 yr
Number of individual NAO^+ events	40 (2.35 yr^{-1})	27 (1.59 yr^{-1})
Number of individual NAO^- events	15 (0.88 yr^{-1})	27 (1.59 yr^{-1})
Number of NAO^- to NAO^+ transition events	11 (0.65 yr^{-1})	6 (0.35 yr^{-1})
Number of NAO^+ to NAO^- transition events	10 (0.59 yr^{-1})	11 (0.65 yr^{-1})

TABLE 2. As in Table 1, but for case 2: P1 is 1978/79–90/91 and P2 is 1991/92–2011/12.

	Epoch	
	P1 = 13 yr	P2 = 21 yr
Number of individual NAO^+ events	26 (2.00 yr^{-1})	41 (1.95 yr^{-1})
Number of individual NAO^- events	15 (1.15 yr^{-1})	27 (1.29 yr^{-1})
Number of NAO^- to NAO^+ transition events	10 (0.77 yr^{-1})	7 (0.33 yr^{-1})
Number of NAO^+ to NAO^- transition events	7 (0.54 yr^{-1})	14 (0.67 yr^{-1})

TABLE 3. As in Table 1, but for case 3: P1 is 1985/86–94/95 and P2 is 1995/96–2004/05.

	Epoch	
	P1 = 10 yr	P2 = 10 yr
Number of individual NAO$^+$ events	27 (2.70 yr^{-1})	15 (1.50 yr^{-1})
Number of individual NAO$^-$ events	5 (0.50 yr^{-1})	11 (1.10 yr^{-1})
Number of NAO$^-$ to NAO$^+$ transition events	5 (0.50 yr^{-1})	6 (0.60 yr^{-1})
Number of NAO$^+$ to NAO$^-$ transition events	6 (0.60 yr^{-1})	8 (0.80 yr^{-1})

4. Decadal relationship between NAO events and European blocking

a. *Composite daily NAO indices*

Since NAO$^+$ (NAO$^-$) events correspond to the enhanced (reduced) frequency of EB events, it is expected that the decadal variations of the EB events in their location, intensity, and duration probably result from changes in the statistics of the EB events associated with individual NAO$^+$, NAO$^-$, and transition events from P1 to P2. To examine the decadal relationship between NAO and EB events, we first identify daily NAO$^+$ and NAO$^-$ events during P1 and P2 and perform the composite of their daily indices. Then, based on the composite daily NAO index, we examine the contribution (or association) of different NAO events to the decadal variation of EB events from P1 to P2.

Because the variation of the winter-mean NAO index from P1 to P2 reflects a time-mean change of daily NAO$^+$, NAO$^-$, and regime transition events in winter from P1 to P2, these events during P1 and P2 should be examined for any changes in their frequency from P1 to P2. An NAO$^+$ (NAO$^-$) event is defined if the daily NAO index has $+1.0$ (-1.0) standard deviation that persists for at least 3 consecutive days. Here, the NAO events are divided into individual (in situ) NAO events and NAO transition events, as done in Luo et al. (2012a,b). Individual NAO events are defined to be events that are not preceded by opposite events, whereas the NAO transition events are defined to include both NAO$^-$ and NAO$^+$ events, in which each event must satisfy the NAO definition. For an NAO$^+$ to NAO$^-$ (NAO$^-$ to NAO$^+$) transition, an NAO$^+$ (NAO$^-$) event must be followed by an NAO$^-$ (NAO$^+$) event. Thus, the regime transition events can be calculated by looking at whether the regime transition condition is satisfied. The detailed definition of NAO transition events can be found in Luo et al. (2012a).

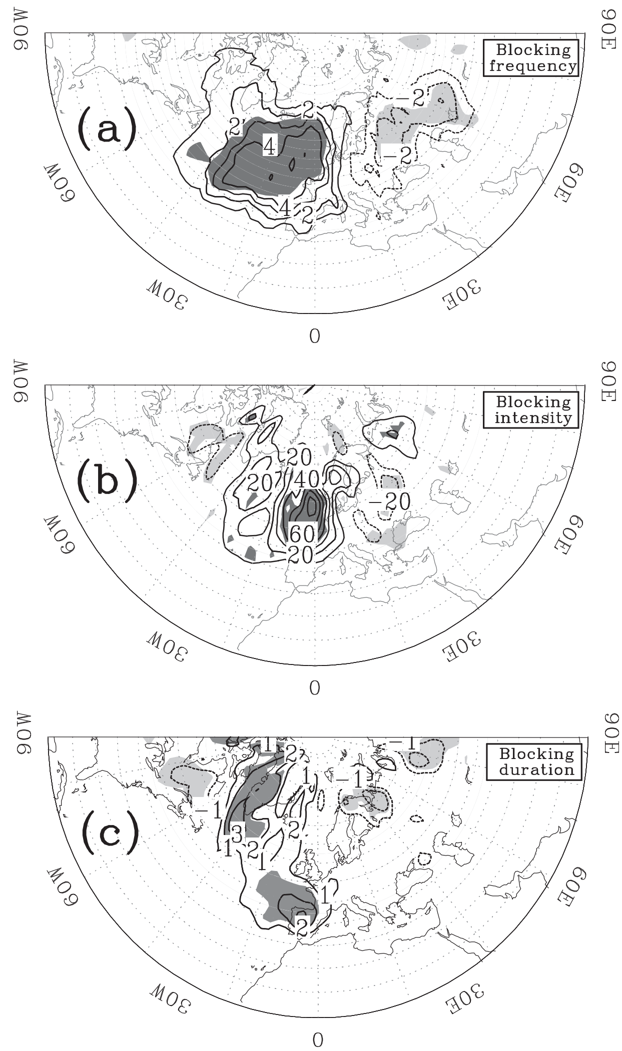

FIG. 6. Epoch (P2 − P1) difference of winter-mean blocking (a) frequency, (b) intensity, and (c) duration between P1 (1978–94) and P2 (1995–2011) based on the blocking index of Diao et al. (2006). The dark (positive) and light (negative) shading denotes the regions above the 95% confidence level for a two-sided Student's *t* test.

In previous studies of Luo et al. (2011, 2012a,b), the role of daily NAO transition events in the increasing/decreasing trends of the winter-mean NAO index has been examined. In the present paper, we will focus on examining the relationship between the decadal variations of EB events and the increasing (decreasing) trends of the winter-mean NAO index during P1 (P2). This study is different from our previous investigations. It is revealed from this study which types of NAO events and background conditions dominate the decadal variations of EB events from P1 to P2.

The event numbers of individual NAO events and transition events are shown in Tables 1–3 for the

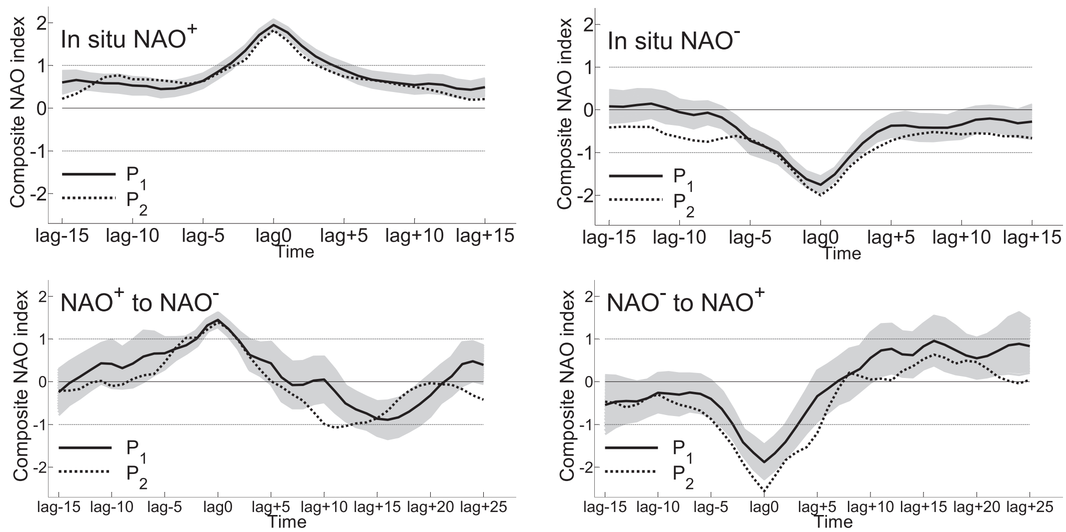

FIG. 7. Time series of the composite daily NAO index of individual (in situ) NAO events and transition events for the periods of P1 (solid) and P2 (dashed). The shading denotes the 90% confidence limit based on a Monte Carlo simulation. The line segments outside the shading area are statistically significant. The solid horizontal line denotes the zero value of the NAO index, and the dashed horizontal line represents one standard deviation value.

different epochs P1 and P2. There are 40 and 27 individual NAO$^+$, 15 and 27 individual NAO$^-$ events, 11 and 6 NAO$^-$ to NAO$^+$ transition events, and 10 and 11 NAO$^+$ to NAO$^-$ transition events during P1 (1978–94) and P2 (1995–2011), respectively. This hints that the frequency of individual NAO$^+$ and NAO$^-$ events exhibits a clear decadal variation from P1 to P2 because of a large difference of their annual-mean frequency between P1 and P2 (Table 1). On the other hand, because the number of NAO$^-$ to NAO$^+$ transition events is almost identical to that of the opposite transition events during P1, individual NAO$^+$ events seem to play a major role in the spatial distribution of EB events compared to individual NAO$^-$ events during P1. However, during P2, NAO$^+$ to NAO$^-$ transition events play an important role in the time-mean distribution of EB events because the frequency of NAO$^+$ to NAO$^-$ transition (individual NAO$^-$) events is much higher than (the same as) that of opposite transition (individual NAO$^+$) events (Table 1).

When 1978–2011 is split into two epochs P1 (1978–90) and P2 (1991–2011), individual NAO$^+$ events are seen to be more frequent than individual NAO$^-$ events for each epoch from their annual-mean values (Table 2). For this case, there are 7 and 14 NAO$^+$ to NAO$^-$ transition events and 10 and 7 NAO$^-$ to NAO$^+$ transition events during P1 and P2. During P2, the frequency of NAO$^+$ to NAO$^-$ transition events is still much higher than that of NAO$^-$ to NAO$^+$ transition events (Table 2). This change in the frequency of NAO transition events from P1 to P2 compensates the frequency change of individual NAO$^+$ events and results in similar P2 − P1 difference patterns, shown in Figs. 5a–c. For two epochs P1 (1985–94) and P2 (1995–2004), the compensation effect of NAO transition events almost vanishes, because the frequency of NAO$^+$ to NAO$^-$ transition events is nearly identical to that of opposite transition events during each epoch (Table 3). In the following discussion, we will focus on examining the case for two epochs: P1 (1978–94) and P2 (1995–2011).

To calculate the IB frequency distribution associated with different types of NAO events, we perform a composite of daily NAO indices for P1 (1978–94) and P2 (1995–2011) in terms of the numbers of individual NAO events and transition events in Table 1 and show the results in Fig. 7. The statistical significance of the difference of the composite daily NAO index between P1 and P2 is also tested using the Monte Carlo method, which is used to test the null hypothesis by generating 1000 random sample points. In this figure, the composite of the daily NAO indices for individual NAO events for each phase is performed, with the peak (largest amplitude) of each event being selected as the lag 0 day. For regime transition events, the composite of their daily NAO indices is made using the peak of NAO$^+$ (NAO$^-$) for NAO$^+$ to NAO$^-$ (NAO$^-$ to NAO$^+$) transition events as lag 0 day. It is seen that for individual NAO events, the composite NAO$^+$ index is higher during P1 than during P2 during the mature stage, while the composite NAO$^-$ index is lower during P2 than during P1. For the transition regimes, the composite NAO index is generally lower (higher) during P2 (P1) than during P1 (P2) as the NAO$^+$ (NAO$^-$) event transitions into a NAO$^-$ (NAO$^+$) event.

Figure 7 shows that the difference in the composite daily NAO indices for individual NAO$^+$ and NAO$^+$ to NAO$^-$ transition events between P1 and P2 is statistically insignificant. However, this does not imply that there is no change in the statistics of the EB events between P1 and P2. This is because the marked variation of the winter-mean NAO index from P1 to P2 mainly reflects the frequency change of individual NAO and transition events between P1 and P2 (Tables 1–3) rather than the difference in the composite daily NAO index between P1 and P2 (Fig. 7). Therefore, the P2 − P1 difference of the composite daily NAO index cannot reflect the frequency changes of the NAO events and, thus, the decadal variation of the EB events from P1 to P2 associated with NAO events. The main reason is that the EB events occur primarily downstream of the NAO region and that they are related to not only the phase of NAO (Luo et al. 2007a), but also its background conditions (Luo and Cha 2012). Thus, it is natural that changes in the winter-mean NAO index that are associated with the EB activity change from P1 to P2 (Fig. 2) are related to not only the changes in the frequencies of daily NAO and regime transition events between P1 and P2 (Tables 1–3), but also the decadal changes of the background conditions from P1 to P2. Conversely, changes in the composite daily NAO index from P1 to P2 may not be important for the decadal variability of EB events.

However, it is convenient for us to calculate the composite IB frequency distributions associated with daily NAO events during P1 and P2 according to the time evolution of the composite daily NAO indices, as shown in Fig. 7. As the time scales of individual NAO events are about 10–20 days (Feldstein 2003) and EB events can occur during days after an NAO$^+$ event peaks, we computed the composite IB frequency averaged from lag −10 to lag +15 days (lag 0 refers to the day when the NAO event peaks) for individual NAO events during P1 and P2 (see Fig. 8). For the transition events, our composite is performed only in the time interval between the days 5 before and after the strongest stage of the NAO$^+$ and NAO$^-$ event associated with the NAO$^+$ to NAO$^-$ and NAO$^-$ to NAO$^+$ transitions (see Fig. 9).

b. *EB frequencies during two phases of individual NAO events*

Figure 8 shows the composite IB frequency in the Euro-Atlantic sector during the whole life cycles of individual NAO$^+$ and NAO$^-$ events during P1 and P2 and its epoch difference. It is seen that during the total process of NAO$^+$ events, the blocking events are mainly distributed along the southwest–northeast (SW–NE) direction over Europe, with a few blocking events over Greenland (Figs. 8a,b). The region with high blocking frequency is notably shifted northeastward during P1 compared to P2, similar to Figs. 3a–d, which were not stratified by the type of NAO events indicated in Tables 1–3 and Fig. 7. The highest blocking frequency during P1 is located over the southwestern side of WE (Fig. 8a). Associated with NAO$^-$ events, the IB frequency in the Euro-Atlantic sector exhibits a southeast–northwest (SE–NW) distribution during P1 and P2 (Figs. 8d,e), and the P2 − P1 difference (Fig. 8f) shows that the blocking frequency is generally higher from Greenland to Europe during P2 than P1. This may be related to the reduced mean westerly winds over the region from the North Atlantic to Europe during P2, as shown below.

The blocking frequency patterns associated with individual NAO$^+$ and NAO$^-$ events shown in Fig. 8 are consistent with previous findings. For example, Croci-Maspoli et al. (2007a) linked the blocking occurrence over Greenland to the negative phase of the NAO. Woollings et al. (2008) suggested that NAO$^-$ (NAO$^+$) may correspond to blocked (unblocked) days over Greenland and the North Atlantic.

For the two phases of individual NAO events, the enhanced-blocking-frequency regions also have enhanced blocking intensity (not shown). Thus, the spatial patterns for the blocking frequency and intensity during P1 and P2 match each other. A comparison between Figs. 3 and 8 suggests that the enhanced blocking frequency over EE during P1 (Fig. 3a) results mainly from the blocking frequency associated with NAO$^+$ events, which are more frequent than NAO$^-$ events during P1 (Table 1). On the other hand, the individual NAO$^+$ and NAO$^-$ events are fairly balanced during P2, as noted below, which would result in a blocking frequency pattern shifted more westward compared to P1, as shown in Fig. 3. Of course, during P2, the westward shift of EB events associated with NAO$^+$ events can increase the frequency of EB events in WE (Figs. 8a–c).

c. *Geographical distribution of the EB frequency for regime transition events*

The physical process for the NAO regime transition has been identified by previous investigators (Luo et al. 2011, 2012b; Michel and Rivière 2011; Michel et al. 2012). It has been revealed that the NAO$^+$ to NAO$^-$ or zonal regime to Greenland anticyclone transitions are accomplished via the preferential transition paths from the zonal regime to Scandinavian blocking (or high-latitude EB) and from Scandinavian blocking to Greenland anticyclone (Michel and Rivière 2011). Thus, it is natural that the variation of EB events is linked to the

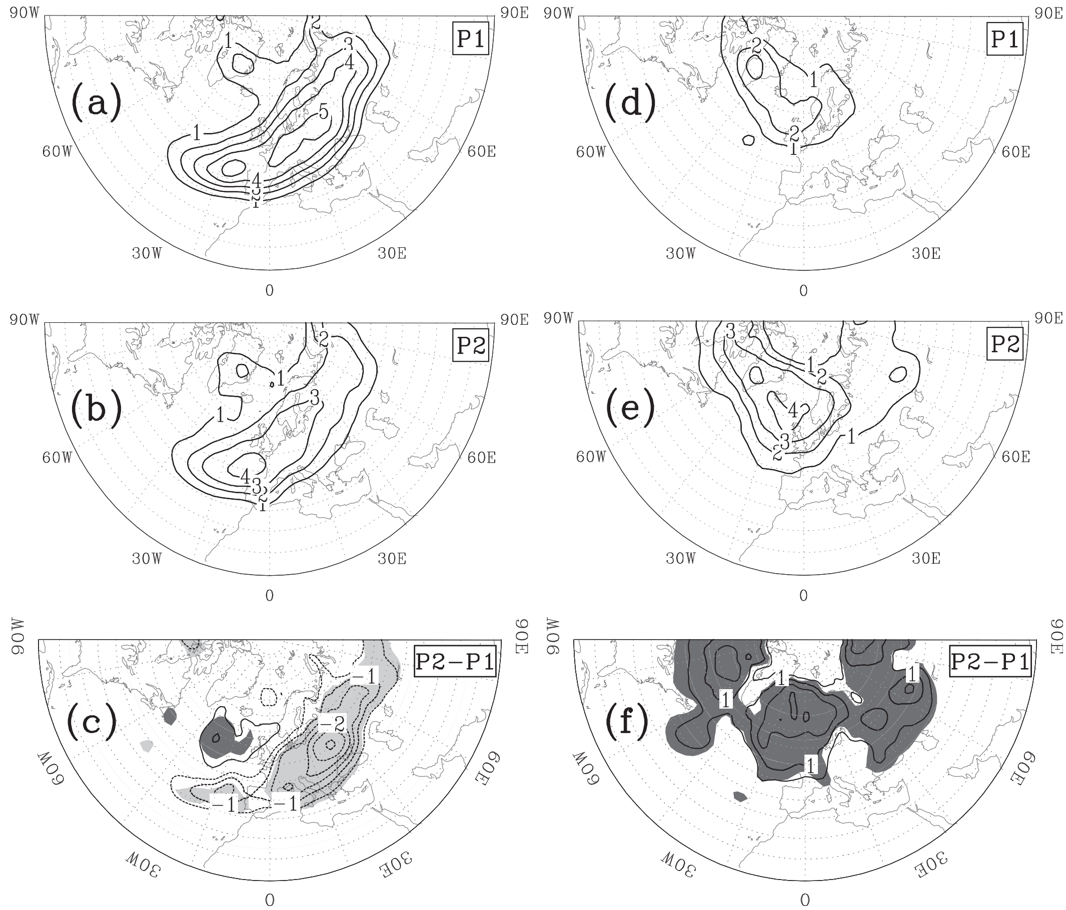

FIG. 8. Geographical distributions of the composite winter instantaneous blocking frequency (%) associated with the individual (a)–(c) NAO$^+$ and (d)–(f) NAO$^-$ events based on the blocking index of Davini et al. (2012b) for (a),(d) P1 (1978–94); (b),(e) P2 (1995–2011); and (c),(f) their difference (P2 − P1). The frequency is expressed as a percentage of the total number of days in the winter (November–March). The shadings denote the regions above the 95% confidence level based on a two-sided Student's t test.

change in regime transition events. Here, we will focus on examining the relationship between the EB activity and NAO transition events on decadal time scales instead of examining the basic physics of the regime transitions (Luo et al. 2012b).

Figure 9 shows the spatial distributions of the composite IB frequency for 17 NAO$^-$ to NAO$^+$ and 21 NAO$^+$ to NAO$^-$ transition events during 1978–2011. This figure reflects the contribution of the regime change of the NAO event to the EB activity, although the frequencies of NAO$^-$ to NAO$^+$ and NAO$^+$ to NAO$^-$ transition events are much lower than those of individual NAO events during 1978–2011. It is interesting to note that the blocking frequency is distributed along the SE–NW direction and is higher over Greenland and northern Europe before the transition of NAO$^-$ events toward NAO$^+$ events (Fig. 9a). However, after the transition, the blocking frequency becomes distributed along the SW–NE direction and shifts northeastward to produce an enhanced blocking frequency in EE and southern Europe (Fig. 9b). This can be clearly seen from the blocking frequency difference between NAO$^+$ and NAO$^-$ events (Fig. 9c). The NAO$^+$ to NAO$^-$ transition events can increase the frequency of blocking events in Greenland and WE (Figs. 9d–f). We also investigated the impact of the sampling number of NAO regime transition events on the composite results and found that the analysis results presented here are insensitive to the sample number of NAO regime transition events (not shown).

The contribution of NAO transition events to the EB activity is negligible during P1 (1978–94), because the frequency of NAO$^-$ to NAO$^+$ transition events is almost identical to that of opposite regime transition events. On the other hand, since the frequency of NAO$^+$ to NAO$^-$ transition events is much higher than that of NAO$^-$ to NAO$^+$ events during P2, NAO$^+$ to NAO$^-$ transition events during P2 enhance the frequency of EB events in WE (Fig. 9f). It is also seen that the spatial

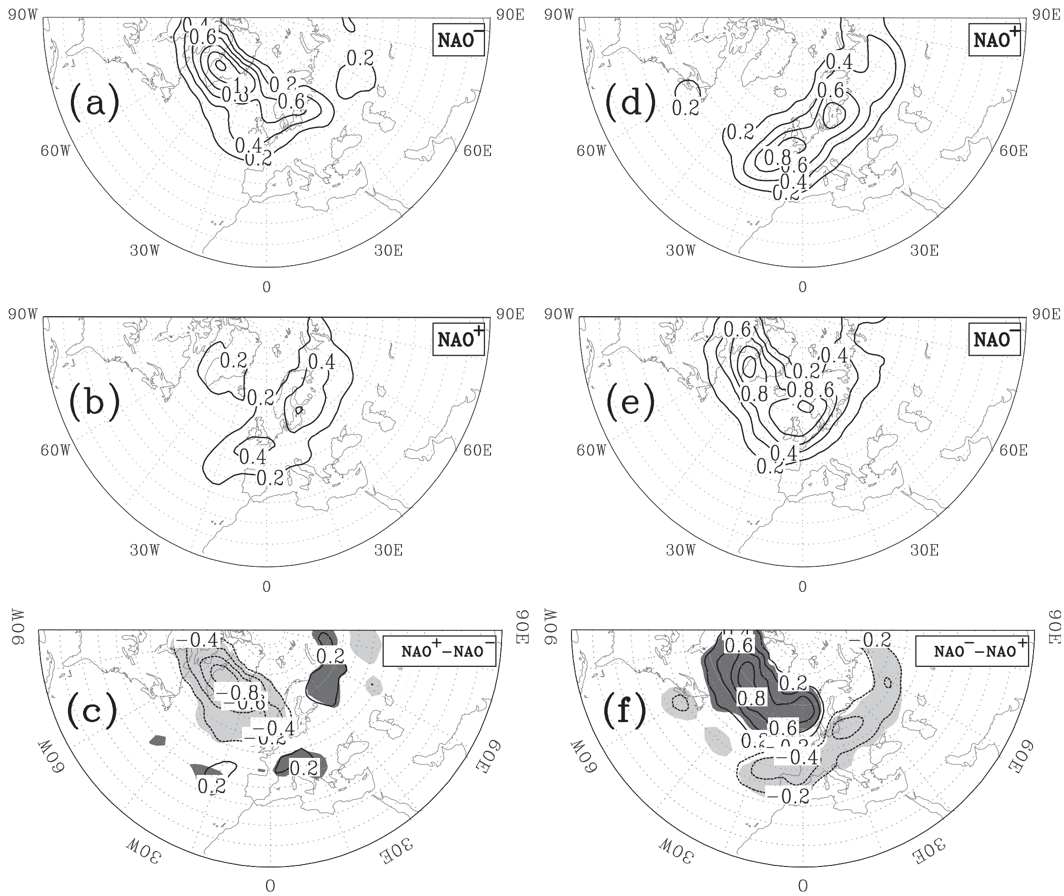

FIG. 9. Geographical distributions of the composite winter instantaneous blocking frequency (%) during the (a),(e) NAO^- and (b),(d) NAO^+ phases and (c),(f) their difference associated with (a)–(c) NAO^- to NAO^+ and (d)–(f) NAO^+ to NAO^- transition events in winter during 1978–2011.

pattern of the blocking frequency during P1 (P2), as shown in Figs. 3a–c is actually equivalent to a superimposition of the blocking frequency distributions associated with individual NAO^+ (Figs. 8a,b), NAO^- (Figs. 8d,e), and regime transition (Fig. 9) events during P1 (P2).

A comparison between Figs. 3, 8, and 9 indicates that the eastward shift of EB events associated with individual NAO^+ events contributes to the enhanced blocking frequency in EE during P1, whereas the enhanced EB events associated with individual NAO^+, NAO^- events and NAO^+ to NAO^- transition events play comparable roles in the enhanced blocking frequency in WE during P2. By contrast, the increased frequency of NAO^+ (NAO^-) events during P1 (P2) is more important for the EB frequency distribution, although the frequency change of NAO transition events has a large effect during P2. As noted below, the significant change in the European blocking activity is closely related to the variation of the Atlantic background conditions from P1 to P2.

In summary, the increased frequencies of individual NAO^- events and NAO^+ to NAO^- transition events during P2 result in an enhanced EB frequency in WE, while the NAO^- to NAO^+ and NAO^+ to NAO^- transition events are fairly balanced during P1, thus making little contribution to the mean EB activity.

5. Temporal relationship between EB events and the phase of NAO

It would be interesting to examine the correlation between the IB frequency index and the daily NAO index in order to understand the relationship between EB events and the phase of the NAO event, although blocking events over northern Europe were found to precede the NAO^- or Greenland blocking events (Feldstein 2003; Woollings and Hoskins 2008; Sung et al. 2011). Here, we will focus on the case of individual NAO events, because a regime transition event is simply considered as a superposition of both individual NAO^- and NAO^+ events.

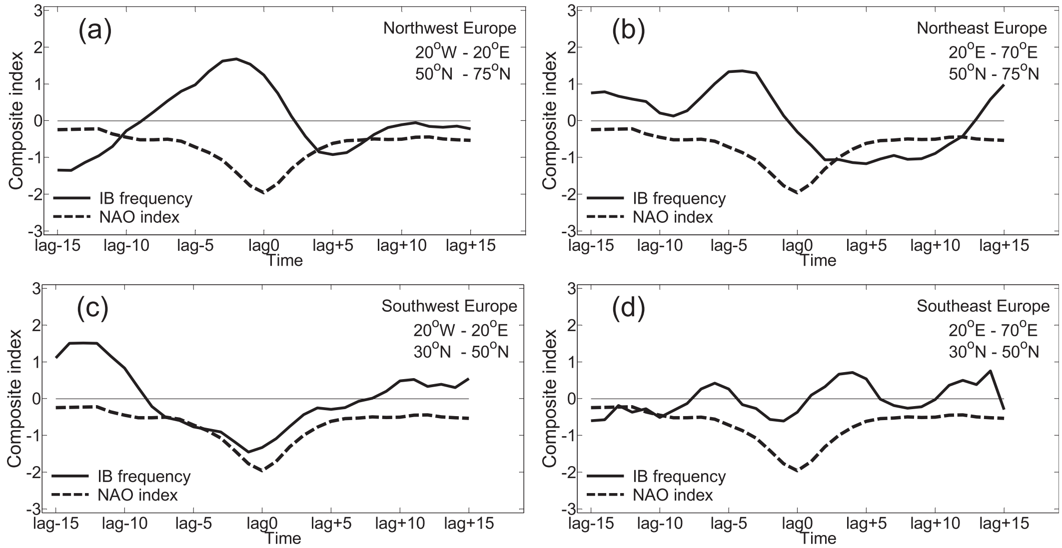

FIG. 10. Temporal evolution of the composite daily NAO (dashed line) and IB frequency indices (solid line) during the life cycle of individual NAO$^-$ events in four regions: (a) northwestern, (b) northeastern, (c) southwestern, and (d) southwestern Europe. The *x*-axis is the lag (days) with lag 0 corresponding to the day when the NAO event peaks. For example, lag −10 (lag +10) corresponds to 10 days before (after) the day when the NAO event peaks.

The time series of the composite daily IB frequency and NAO indices in four regions: northwestern (50°–75°N, 20°W–20°E), northeastern (50°–75°N, 20°–70°E), southwestern (30°–50°N, 20°W–20°E), and southeastern (30°–50°N, 20°–70°E) Europe are shown in Fig. 10 for the NAO$^-$ events and in Fig. 11 for the NAO$^+$ events. The north–south partition of the European continent is based on the fact that the zero line between anticyclonic and cyclonic anomalies for the two NAO phases is located near 50°N (Luo et al. 2012b, their Fig. 1). It is seen from Fig. 10 that during the period from lag −10 to lag +10 days, the composite daily blocking frequency index exhibits negative correlations with the daily NAO$^-$ index, with a correlation coefficient *r* of −0.89 at a 1-day lead (by blocking) over northwestern Europe and −0.72 at a 4-day lead over northeastern Europe (Figs. 10a,b). Over southwestern Europe or the eastern Atlantic, the composite daily IB frequency index shows a positive correlation of 0.72 with the daily NAO$^-$ index at a 1-day lead (Fig. 10c). However, over southeastern Europe, the correlation is significant at a 3-day lead only during the period from lag −5 to lag +5 days (Fig. 10d). These

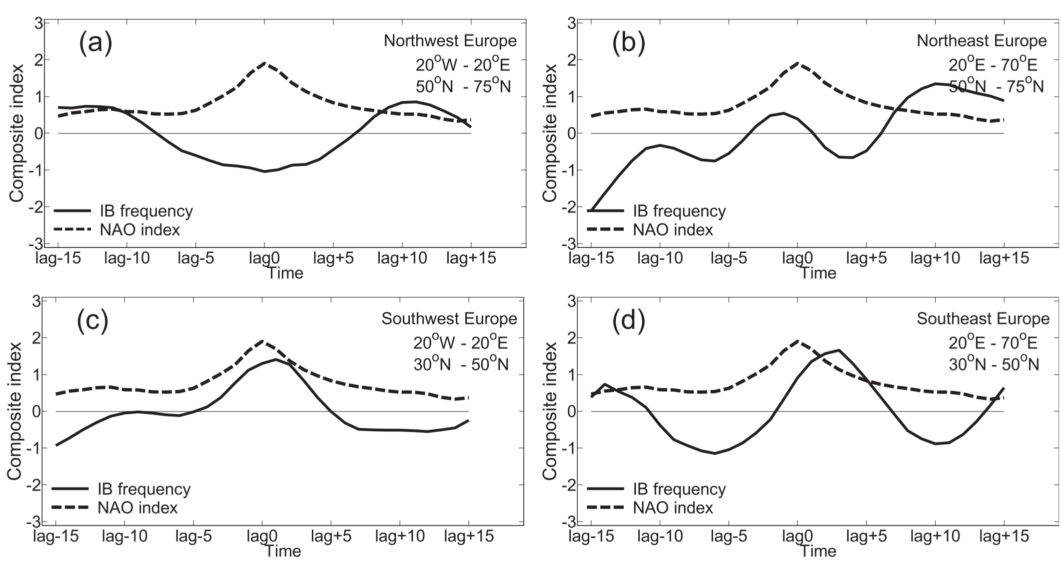

FIG. 11. As in Fig. 10, but for individual NAO$^+$ events.

results are consistent with previous findings (Feldstein 2003; Woollings et al. 2008; Sung et al. 2011) that NAO$^-$ events result from the retrogression (i.e., westward migration) of amplifying blocks initiated over northern Europe.

We can further see from Fig. 11 that during the period from lag -10 to lag $+10$ days, the composite daily blocking frequency index is correlated with the composite daily NAO$^+$ index with $r = 0.77$ at a 1-day lag (by blocking) over southwestern Europe, 0.89 at a 3-day lag over southeastern Europe, -0.61 at a 2-day lag over northwestern Europe, and 0.42 at 2-day lead over northeastern Europe. Also, the increased EB frequency over northeastern Europe from lag -3 to lag $+1$ day is related to the marked northeastward extension of the amplified anticyclonic anomaly, as seen in Fig. 1a of Luo et al. (2012b). Interestingly, the blocking frequency over northwestern and northeastern Europe (Figs. 11a,b) is notably enhanced after a long decay of the NAO$^+$ event. Because the time that the blocking frequency reaches a maximum is shorter for southern Europe than for northern Europe, we conclude that the enhanced EB frequency over southern Europe is more likely to be a direct result of the eastward shift of the amplified anticyclonic anomaly of the composite NAO$^+$ anomaly (Fig. 1a of Luo et al. 2012b). However, the reintensified EB frequency over northern Europe after a long decay of the NAO$^+$ event is probably due to energy dispersion of Rossby waves. Even so, the result here suggests that NAO$^+$ events precede EB events. In other words, EB events may result from individual NAO$^+$ events. Although individual NAO$^-$ events correspond to an enhanced frequency of EB events in WE, the results shown in Figs. 8a–c indicate that the change in the time-mean EB events associated with individual NAO$^+$ events from P2 to P1 seems to play a dominant role in the decadal eastward shifts of EB events. As revealed below, the lead–lag relationship between the phase of NAO and EB events is closely related to the westward (eastward) displacement of the NAO$^-$ (NAO$^+$) dipole anomaly.

The above relationship between the NAO and EB events can also be explained in terms of the westward (eastward) shift of the composite daily NAO$^-$ (NAO$^+$) dipole anomaly, as shown in Fig. 1 of Luo et al. (2012b). For the negative phase (Luo et al. 2012b, their Fig. 1b) a weak dipole with an anticyclonic anomaly to the north of a cyclonic anomaly is located over northern Europe during the beginning stage (from lag -6 to lag -4 days). The dipole anomaly retrogrades as it intensifies and then leads to the establishment of an NAO$^-$ anomaly. Sung et al. (2011) also found that NAO$^-$ events originate from the westward drifting of amplifying blocking ridges over northern Europe. This implies that the existence of blocking events over northern Europe is a precondition for the development of individual NAO$^-$ events (Feldstein 2003; Woollings et al. 2008; Sung et al. 2011). Thus, it is argued that the EB event precedes the individual NAO$^-$ event. For the positive phase, at the beginning stage (from lag -8 to lag -6 days) of an NAO$^+$ anomaly, a weak dipole with a large-scale cyclonic anomaly to the north of an anticyclonic anomaly is located over Greenland (Luo et al. 2012b, their Fig. 1a). An individual NAO$^+$ event can form because of the amplification of the dipole anomalies, which expand eastward. The northeastward expansion of the intensified anticyclonic anomaly over the southern side of the North Atlantic basin can lead to an enhanced anticyclonic anomaly over southern and northeastern Europe. This may be a reason why the EB events over southwestern and southeastern Europe have the stronger IB frequency after the daily NAO$^+$ index reaches a maximum at lag 0 days (Figs. 11c,d). However, after a long decay of the individual NAO$^+$ event, the anticyclonic anomaly over northern Europe is reintensified (Luo et al. 2012b, their Fig. 1a) so that there is a reenhanced EB frequency over northwestern and northeastern Europe after the NAO$^+$ decay (Figs. 10a–b). Thus, individual NAO$^+$ events precede EB events. Roughly speaking, EB events can be considered as a forcing of NAO$^-$ events, whereas the NAO$^+$ events can be understood as a forcing of EB events.

The composite wind fields (not shown) further revealed that the strengthening (weakening) of the zonal wind at middle to high latitudes over the Atlantic basin is concomitant with the establishment of the NAO$^+$ (NAO$^-$) dipole anomaly (Luo et al. 2007b). As a result, the westward (eastward) displacement of individual NAO$^-$ (NAO$^+$) dipole anomalies is a self-maintaining phenomenon as a response to the reduced (enhanced) mean zonal wind in the mid- to high-latitude region. Woollings et al. (2008) identified a daily blocking event over Greenland or the North Atlantic as a daily NAO$^-$ event. Here, we define a daily anticyclonic anomaly over the European continent as a daily EB event. If an anticyclonic anomaly is located in high (low) latitudes over Europe or the Atlantic basin, the daily anticyclonic anomaly is referred to as a daily EB event over northern (southern) Europe or a daily NAO$^-$ (NAO$^+$) event. Because the anticyclonic anomaly of the individual NAO$^+$ (NAO$^-$) pattern is located in lower (higher) latitudes, the eastward (westward) shift of the NAO$^+$ (NAO$^-$) pattern can increase (decrease) the frequency of EB events over southern (northern) Europe. Therefore, the zonal movement of the NAO$^+$ (NAO$^-$) anomaly provides a partial explanation for why an NAO$^+$ (NAO$^-$) event leads (lags) the EB event over southern (northern) Europe, as shown in Fig. 11 (Fig. 10). However, the frequency variation of EB events over northeastern Europe cannot be entirely explained in terms of the eastward (westward) expansion of the anticyclonic anomalies of the NAO^+ (NAO^-) pattern, because it is difficult for the anticyclonic anomaly of the NAO pattern to reach northeastern Europe unless a local amplification of blocking ridges takes place over northeastern Europe. Further theoretical investigation on this problem will be presented in Part II using a nonlinear multiscale interaction (NMI) model developed by Luo et al. (2007b) and Luo and Cha (2012).

6. Atlantic conditions affecting decadal shifts of European blocking events

In recent years, the occurrence of NAO events has been identified to be related to the synoptic Rossby wave breaking (RWB) in the Atlantic storm-track region (Benedict et al. 2004; Franzke et al. 2004; Rivière and Orlanski 2007; Strong and Magnusdottir 2008; Woollings et al. 2008). While the phase of NAO events is dominated by the form of RWB (Benedict et al. 2004; Franzke et al. 2004; Rivière and Orlanski 2007), it was also found to be related to the speed, position, and the north–south shift of the Atlantic jet stream (Woollings et al. 2010a,b; Woollings and Blackburn 2012; Davini et al. 2012a). Luo et al. (2008) found in a theoretical model that the latitudinal position of the jet core of the Atlantic jet stream prior to the NAO onset determines the phase of the subsequent NAO event. When the jet core shifts northward (southward), the eddy-driven NAO^+ (NAO^-) anomaly intensifies (Luo et al. 2008, their Figs. 6b and 8b). Our calculations revealed (not shown) that there exist an increasing (decreasing) northward position of the Atlantic jet core during P1 (P2), which is likely an important cause for an intensified (weakened) NAO^+ anomaly and its increased (decreased) frequency during P1 (P2), leading to the increasing (decreasing) trend of the winter-mean NAO index during these periods. Although Luo and Cha (2012) examined the decadal phase relationship between decadal variations in the Atlantic jet and NAO, the fine relationship of the increasing (decreasing) trend of the winter-mean NAO index with the decadal position of the Atlantic jet core is still unclear. This deserves a separate study.

Häkkinen et al. (2011) found that the variability of Euro-Atlantic blocking over years to several decades is correlated with the Atlantic Ocean surface temperature and with significant changes in Atlantic Ocean circulation. Thus, it is possible that decadal variability of atmospheric blocking events in the Euro-Atlantic sector is related to decadal variations of the mean westerly wind and storm track over the Atlantic basin due to the effects of recent changes in ocean surface temperature and Atlantic Ocean circulation. In the present paper, we propose a new view: that the decadal variation of EB events results from the decadal NAO variability because of the decadal jet and Atlantic storm-track variabilities.

Since there is a strong coupling between the NAO event, the Atlantic storm track, and the North Atlantic jet stream (Lau 1988), clearly identifying their causal relationship is difficult. However, if we can remove the effect of NAO events on the atmospheric basic state during P1 and P2, the variations of the remaining mean wind and storm track from P1 to P2 may reflect the variability and change of atmospheric basic state associated with (but without the effect through NAO) Atlantic Ocean surface temperature, sea ice conditions, and greenhouse gas concentrations, rather than because of a frequency change in NAO events from P1 to P2. Such a basic state may be considered as the background state of the NAO event, although the westerly wind and storm-track changes associated with the NAO event could be the dominant signals during its evolution. Such background conditions are referred to as ‘‘Atlantic conditions’’ herein.

Here, we define the storm track using the 2.5–7-day EKE at 300 hPa obtained using the second-order Butterworth bandpass filter (Hamming 1989). The P2 − P1 difference of the winter-mean zonal wind and EKE between P1 and P2 is shown for the cases of NAO events excluded (Figs. 12a,c) and included (Figs. 12b,d). In this figure, the calculation of the time-mean zonal wind and EKE is made only within the time range outside the period when individual NAO and regime transition events take place so that the impact of NAO events can be approximately excluded. It is clear that the P2 − P1 difference of the winter-mean zonal wind exhibits positive values at high and subtropical latitudes and negative values at midlatitudes over the North Atlantic, which crudely reflects a decadal change in the mean zonal wind from P1 to P2. Overall, the winter-mean zonal wind averaged over the Atlantic basin is stronger during P1 than during P2 (Fig. 12a). In particular, the enhanced mean zonal wind extends northeastward into northern Europe during P1. The enhancement of the zonal wind during P1 becomes more evident if the zonal winds associated with individual NAO events are included in the calculation (Fig. 12b). This is because the frequency of individual NAO^+ events is higher than (the same as) that of individual NAO^- events during P1 (P2) so that the enhanced mean zonal wind is more evident during P1 than during P2 because of the enhancement of the zonal wind at middle to high latitudes during the NAO^+ episodes. However, the time-mean effect of

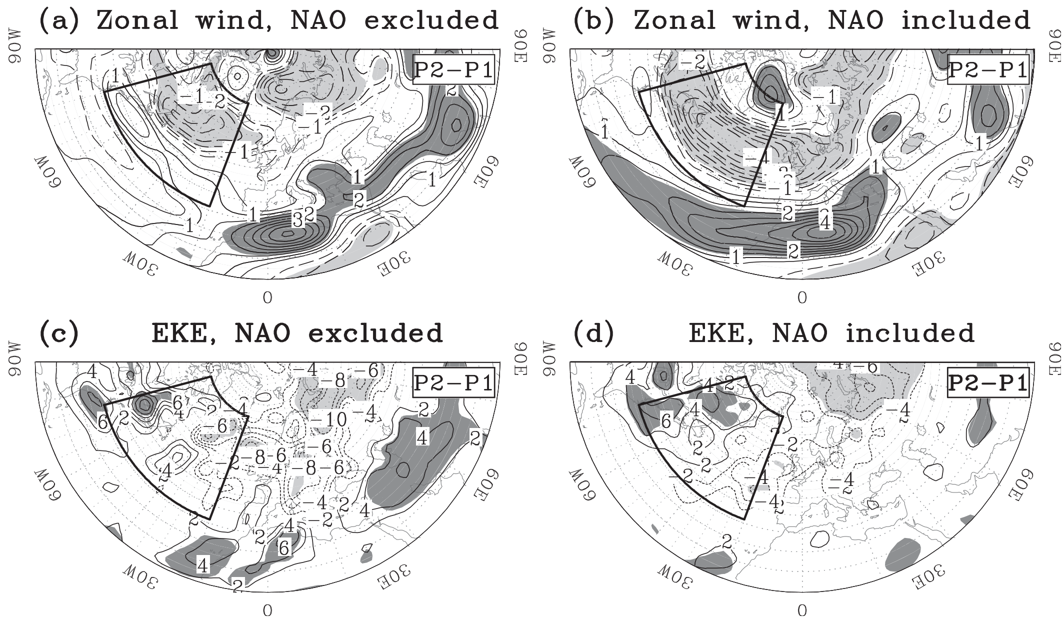

FIG. 12. Epoch (P2 − P1) difference of the winter-mean (a),(b) zonal wind and (c),(d) EKE in the Euro-Atlantic sector between P1 (1978–94) and P2 (1995–2011). Zonal wind–associated NAO events have been removed in (a) and (c) and retained in (b) and (d). The square denotes the Atlantic basin. The shadings denote the regions above the 95% confidence level based on a two-sided Student's *t* test.

regime transition events does not induce such an obvious variation because of the near offset between the NAO^+ and NAO^- events within the NAO transition events (not shown).

Furthermore, we can see in Fig. 12c that over the western North Atlantic basin and its upstream side, the P2 − P1 difference of the EKE exhibits a large positive-value region. This reflects a significant decadal change of the Atlantic storm-track strength, which suggests that the western Atlantic storm track is stronger during P2 than during P1. This feature can also be seen when zonal winds associated with individual NAO events are included (Fig. 12d). Thus, the change in the western Atlantic storm-track strength from P1 to P2 is likely to be another important factor affecting the decadal change of the EB events from P1 to P2. As noted by Luo et al. (2012b), the reduced Atlantic mean zonal wind (enhanced western Atlantic storm track) strength favors the frequent occurrence of NAO^+ to NAO^- transition events. Even so, weaker Atlantic mean zonal wind and stronger western Atlantic storm-track strengths observed during P2 are conducive to the enhanced blocking frequency in WE, because the local increase in EB events associated with individual NAO^- events can occur during P2 (Figs. 8d–f). Of course, such an enhanced blocking frequency in WE is also tied to the westward migration of EB events associated with individual NAO^+ and NAO^+ to NAO^- transition events during P2 (Figs. 9d–f).

To further understand the impact of the Atlantic background conditions on the zonal position of EB events, we define the zonal wind and EKE averaged from lag −20 to lag −10 days and over the region 40°–70°N, 70°W–0° (40°–70°N, 75°–30°W) for all individual NAO^+ events as the Atlantic mean zonal wind (western Atlantic storm track) strength prior to the NAO onset or approximately define them as the Atlantic conditions without NAO events included. The mean zonal wind (western Atlantic storm track) strength is represented by its anomaly or deviation from its mean value for all NAO^+ events. Furthermore, the longitude, where the maximum blocking intensity of an EB event is located, is defined as the blocking position during its life cycle. Here, we consider the case of individual NAO^+ events because their frequency is higher than that of individual NAO^- events during 1978–2011. On the other hand, the result of individual NAO^- events is easily obtained, because individual NAO^- events correspond to blocking events.

Figures 13a and 13b show the longitude of the blocking position during NAO^+ episodes versus the normalized Atlantic mean zonal wind and western Atlantic storm-track strengths prior to the NAO onset. It is seen that the EB events tend to occur in eastern (western) Europe as the Atlantic mean zonal wind strength prior to the NAO onset is enhanced (reduced) (Fig. 13a), hence implying that the stronger (weaker) the mean westerly wind or jet strength, the more EB events in EE (WE). Figure 13b also

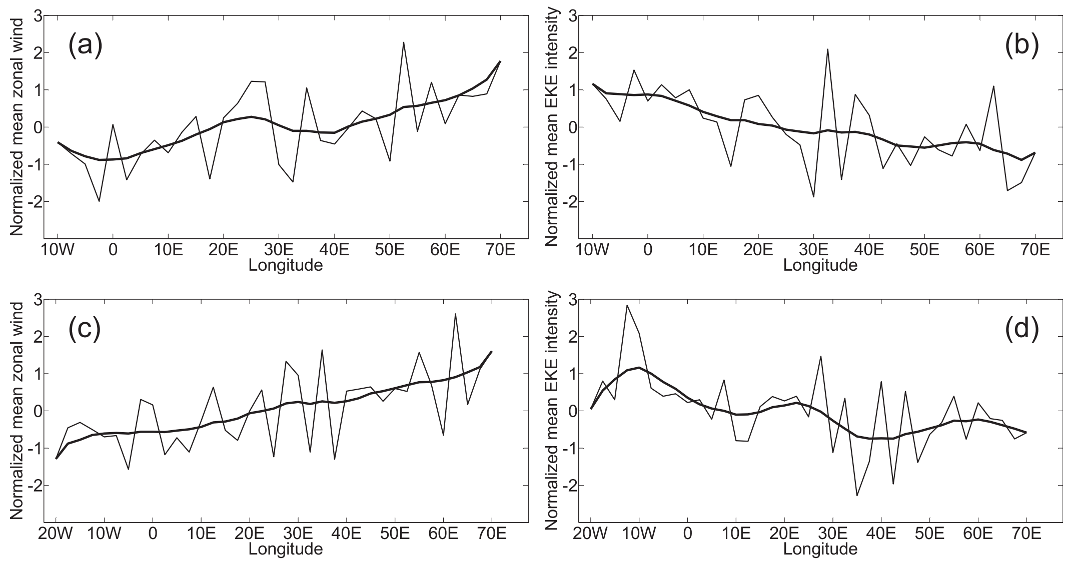

FIG. 13. Longitude of the blocking position associated with individual NAO$^+$ events versus normalized mean zonal wind and EKE strength averaged (a),(b) from lag −20 to lag −10 days prior to the NAO onset and (c),(d) from lag −10 to lag +10 days during the NAO$^+$ episodes. The blocking position with the mean (a),(c) zonal wind and (b),(d) EKE strengths. The thick line denotes a nine-point smoothing curve.

shows that the center of the EB events associated with individual NAO$^+$ events shifts westward (eastward) as the western Atlantic storm track becomes stronger (weaker) prior to the NAO onset. If the averaging period is changed to the case from lag −10 to lag +10 days, the results are similar (Figs. 13c,d). Further, the intensity and duration of EB events are found to exhibit similar variations with Atlantic zonal winds and storm-track strength (not shown). Thus, the decadal changes in NAO$^+$ (Table 1) and EB events (Figs. 3 and 4) from P1 to P2 are likely linked to the decadal changes in the strengths of the mean zonal wind in the North Atlantic and western Atlantic storm track, as shown in Fig. 13.

7. Conclusions and discussion

In this paper, we have examined the recent decadal variations of European blocking (EB) events in relation to a change in the winter-mean NAO index from an increasing and high [P1 (1978–94)] to a decreasing and low [P2 (1995–2011)] NAO index period during 1978–2011. To examine the sensitivity of the results to the definition of the subperiods P1 and P2, we also split the period 1978–2011 into two other different epochs: P1 (1978–90) and P2 (1991–2011) and P1 (1985–94) and P2 (1995–2004). It is shown that the results are similar for the three cases. Moreover, our results are found to be insensitive to the choice of the two-dimensional blocking index and reanalysis data.

It is found that there are more intense and persistent EB events in eastern Europe (EE) during P1 than during P2, while the EB events are concentrated more in western Europe (WE) during P2 than during P1. The cause of this decadal shift in the EB event was investigated by examining the EB frequency patterns associated with different types of NAO events and the associated Atlantic background conditions. It is revealed that the decadal change in the EB events from P1 to P2 is closely related to the changes in the different types of the individual NAO events under different Atlantic background conditions, which include the strength of the mean zonal wind and western Atlantic storm track. Specifically, there are more NAO$^+$ (NAO$^-$) events during P1 (P2) associated with stronger (weaker) Atlantic mean zonal wind and weaker (stronger) western Atlantic storm track observed during P1 (P2). Because the EB events associated with NAO$^+$ events extend more eastward in the presence of stronger mean zonal wind during P1 than during P2 (Figs. 13a,b), the decadal changes in the number of NAO$^+$ events from P1 to P2 lead to a westward displacement of the EB events, thus resulting in more EB frequencies in EE during P1. However, a local increase in the frequency of EB events associated with individual NAO$^-$ events related to both weak mean zonal wind and strong western Atlantic storm track and a westward migration of EB events associated with individual NAO$^+$ and NAO$^+$ to NAO$^-$ transition events can lead to an enhanced blocking frequency in WE during P2. Moreover, whether the enhanced frequency of

EB events occurs in eastern (western) Europe is found to be associated with the frequency of NAO^- to NAO^+ (NAO^+ to NAO^-) transition events. However, when the frequency of NAO^- to NAO^+ transition events is almost identical to that of NAO^+ to NAO^- transition events during P1 (Tables 1 and 2), two opposite phases within each transition event would almost offset any impacts and result in a small net effect by these NAO transition events, creating a small decadal variation (Fig. 9). Although the decadal variation of EB events associated with individual NAO events from P1 to P2 is most evident (Fig. 8), the NAO^+ to NAO^- transition–induced decadal change can also be seen during P2, because P2 includes more NAO^+ to NAO^- transition events (Tables 1 and 2).

Moreover, our study also reveals that the existence of blocking events over northern Europe is a precondition for the development of individual NAO^- events, while the existence of NAO^+ events is a favorable condition for the enhanced frequency of EB events over Europe, especially over southern Europe.

Different from our previous findings (Luo et al. (2011; 2012a,b), in this paper we present new results that the decadal shift of EB events is caused by or associated with the frequency change in individual NAO^+, NAO^-, and regime transition events. The frequency change of the NAO events contributes to the decadal variation of the winter-mean NAO index from P1 to P2 through the change of Atlantic background conditions (i.e., winter-mean zonal wind and storm-track strengths in the Atlantic basin) from P1 to P2. In particular, the distribution of EB events during P2 is also significantly affected by the increased NAO^+ to NAO^- transition events.

On the other hand, although we have examined the relationship between NAO and EB events during P1 to P2, the impact of the east Atlantic (EA) pattern on the EB event is not explored. However, as noted by many investigators, the combination of NAO and EA patterns can explain changes in the jet speed, while the NAO pattern can represent jet shifts (Woollings et al. 2010a,b; Hurrell and Deser 2009; Woollings and Blackburn 2012). Since the variability of the Atlantic jet can modulate the blocking activity in the Euro-Atlantic sector (De Vries et al. 2013), it is argued that changes in the EA pattern can affect the Euro-Atlantic blocking activity in intensity, duration, and location through altering the Atlantic jet. Even so, our results are tenable because the EA pattern is a secondary empirical orthogonal function (EOF) mode. Nevertheless, the role of EA patterns in the variation of EB events should be examined in future studies.

At present, although the eddy straining mechanism (Shutts 1983) and selective absorption mechanism (Yamazaki and Itoh 2013) models have been proposed to explain how synoptic eddies excite and maintain a blocking flow, it may be difficult to use these mechanisms to identify the dynamical relationship between the NAO and EB events because NAO events are not involved in these models. In Part II, we will apply a simplified nonlinear multiscale interaction model of NAO events developed by Luo et al. (2007) and Luo and Cha (2012) to examine the dynamical mechanism through which the Atlantic conditions affect EB events associated with individual NAO and transition events.

Acknowledgments. The authors acknowledge support from the National Science Foundation of China (41430533, 41375067, and 41490642) and the "One Hundred Talents Plan" of the Chinese Academy of Sciences (Y163011).

REFERENCES

Barnes, E., J. Slingo, and T. Woollings, 2012: A methodology for the comparison of blocking climatologies across indices, models and climate scenarios. *Climate Dyn.,* **38,** 2467–2481, doi:10.1007/s00382-011-1243-6.

Barriopedro, D., R. García-Herrera, A. R. Lupo, and E. Hernández, 2006: A climatology of Northern Hemisphere blocking. *J. Climate,* **19,** 1042–1063, doi:10.1175/JCLI3678.1.

——, ——, and R. M. Trigo, 2010: Application of blocking diagnosis methods to General Circulation Models. Part I: A novel detection scheme. *Climate Dyn.,* **35,** 1373–1391, doi:10.1007/s00382-010-0767-5.

Benedict, J., S. Lee, and S. B. Feldstein, 2004: Synoptic view of the North Atlantic Oscillation. *J. Atmos. Sci.,* **61,** 121–144, doi:10.1175/1520-0469(2004)061<0121:SVOTNA>2.0.CO;2.

Berggren, R., B. Bolin, and C.-G. Rossby, 1949: An aerological study of zonal motion, its perturbations and break-down. *Tellus,* **1A,** 14–37, doi:10.1111/j.2153-3490.1949.tb01257.x.

Buehler, T., C. C. Raible, and T. F. Stocker, 2011: The relationship of winter season North Atlantic blocking frequencies to extreme cold or dry spells in the ERA-40. *Tellus,* **63A,** 212–222, doi:10.1111/j.1600-0870.2010.00492.x.

Cattiaux, J. R. Vautard, C. Cassou, P. Yiou, V. Masson-Delmontte, and F. Codron, 2010: Winter 2010 in Europe: A cold extreme in a warming climate. *Geophys. Res. Lett.,* **37,** L20704, doi:10.1029/2010GL044613.

Chen, T. C., and J. H. Yoon, 2002: Interdecadal variations of the North Pacific wintertime blocking. *Mon. Wea. Rev.,* **130,** 3136–3143, doi:10.1175/1520-0493(2002)130<3136:IVOTNP>2.0.CO;2.

Cohen, J., and M. Barlow, 2005: The NAO, the AO, and global warming: How closely related? *J. Climate,* **18,** 4498–4513, doi:10.1175/JCLI3530.1.

Croci-Maspoli, M., C. Schwierz, and H. C. Davies, 2007a: Atmospheric blocking: Space-time links to the NAO and PNA. *Climate Dyn.,* **29,** 713–725, doi:10.1007/s00382-007-0259-4.

——, ——, and ——, 2007b: A multifaceted climatology of atmospheric blocking and its recent linear trend. *J. Climate,* **20,** 633–649, doi:10.1175/JCLI4029.1.

Dai, A., H. Li, Y. Sun, L.-C. Hong, LinHo, C. Chou, and T. Zhou, 2013: The relative roles of upper and lower tropospheric thermal contrasts and tropical influences in driving Asian summer monsoons. *J. Geophys. Res. Atmos.,* **118,** 7024–7045, doi:10.1002/jgrd.50565.

Davini, P., C. Cagnazzo, S. Gualdi, and A. Navarra, 2012a: Bidimensional diagnostics, variability, and trends of Northern

Hemisphere blocking. *J. Climate,* **25,** 6496–6509, doi:10.1175/JCLI-D-12-00032.1.

——, ——, R. Neale, and J. Tribbia, 2012b: Coupling between Greenland blocking and the North Atlantic Oscillation pattern. *Geophys. Res. Lett.,* **39,** L14701, doi:10.1029/2012GL052315.

De Vries, H., T. Woollings, J. Anstey, R. J. Haarsma, and W. Hazeleger, 2013: Atmospheric blocking and its relation to jet changes in a future climate. *Climate Dyn.,* **41,** 2643–2654, doi:10.1007/s00382-013-1699-7.

Diao, Y., J. Li, and D. Luo, 2006: A new blocking index and its application: Blocking action in the Northern Hemisphere. *J. Climate,* **19,** 4819–4839, doi:10.1175/JCLI3886.1.

Feldstein, S. B., 2003: The dynamics of NAO teleconnection pattern growth and decay. *Quart. J. Roy. Meteor. Soc.,* **129,** 901–924, doi:10.1256/qj.02.76.

Franzke, C., S. Lee, and S. B. Feldstein, 2004: Is the North Atlantic Oscillation a breaking wave? *J. Atmos. Sci.,* **61,** 145–160, doi:10.1175/1520-0469(2004)061<0145:ITNAOA>2.0.CO;2.

Häkkinen, S., P. B. Rhines, and D. L. Worthen, 2011: Atmospheric blocking and Atlantic multidecadal ocean variability. *Science,* **334,** 655–659, doi:10.1126/science.1205683.

Hamming, R. W., 1989: *Digital Filters.* 3rd ed. Prentice-Hall, 284 pp.

Hurrell, J. W., 1995: Decadal trends in the North Atlantic Oscillation: Regional temperature and precipitation. *Science,* **269,** 676–679, doi:10.1126/science.269.5224.676.

——, and C. Deser, 2009: North Atlantic climate variability: The role of the North Atlantic Oscillation. *J. Mar. Syst.,* **78,** 28–41, doi:10.1016/j.jmarsys.2008.11.026.

Kalnay, E., and Coauthors, 1996: The NCEP/NCAR 40-Year Reanalysis Project. *Bull. Amer. Meteor. Soc.,* **77,** 437–471, doi:10.1175/1520-0477(1996)077,0437:TNYRP.2.0.CO;2.

Lau, N. C., 1988: Variability of the observed midlatitude storm tracks in relation to low-frequency changes in the circulation pattern. *J. Atmos. Sci.,* **45,** 2718–2743, doi:10.1175/1520-0469(1988)045<2718:VOTOMS>2.0.CO;2.

Lejenäs, H., and H. Økland, 1983: Characteristics of Northern Hemisphere blocking as determined from a long time series of observational data. *Tellus,* **35A,** 350–362, doi:10.1111/j.1600-0870.1983.tb00210.x.

Livezey, R. E., and W. Y. Chen, 1983: Statistical field significance and its determination by Monte Carlo techniques. *Mon. Wea. Rev.,* **111,** 46–59, doi:10.1175/1520-0493(1983)111<0046:SFSAID>2.0.CO;2.

Luo, D., and J. Cha, 2012: The North Atlantic Oscillation and North Atlantic jet variability: Precursors to NAO regimes and transitions. *J. Atmos. Sci.,* **69,** 3763–3787, doi:10.1175/JAS-D-12-098.1.

——, A. Lupo, and H. Wan, 2007a: Dynamics of eddy-driven low frequency dipole modes. Part I: A simple model of North Atlantic Oscillations. *J. Atmos. Sci.,* **64,** 3–38, doi:10.1175/JAS3818.1.

——, T. Gong, and Y. Diao, 2007b: Dynamics of eddy-driven low-frequency dipole modes. Part III: Meridional displacement of westerly jet anomalies during two phases of NAO. *J. Atmos. Sci.,* **64,** 3232–3248, doi:10.1175/JAS3998.1.

——, ——, and L. Zhong, 2008: Dynamical relationship between the phase of North Atlantic Oscillations and the meridional excursion of a preexisting jet: An analytical study. *J. Atmos. Sci.,* **65,** 1838–1858, doi:10.1175/2007JAS2560.1.

——, Y. Diao, and S. B. Feldstein, 2011: The variability of the Atlantic storm track and the North Atlantic Oscillation: A link between intraseasonal and interannual variability. *J. Atmos. Sci.,* **68,** 577–601, doi:10.1175/2010JAS3579.1.

——, J. Cha, and S. B. Feldstein, 2012a: Weather regime transitions and the interannual variability of the North Atlantic Oscillation. Part I: A likely connection. *J. Atmos. Sci.,* **69,** 2329–2346, doi:10.1175/JAS-D-11-0289.1.

——, ——, and ——, 2012b: Weather regime transitions and the interannual variability of the North Atlantic Oscillation. Part II: Dynamical processes. *J. Atmos. Sci.,* **69,** 2347–2363, doi:10.1175/JAS-D-11-0290.1.

——, Y. Yao, and A. Dai, 2015: Decadal relationship between European blocking and North Atlantic Oscillation during 1978–2011. Part II: A theoretical model study. *J. Atmos. Sci.,* **72,** 1174–1199, doi:10.1175/JAS-D-14-0040.1.

Michel, C., and G. Rivière, 2011: The link between Rossby wave breakings and weather regime transitions. *J. Atmos. Sci.,* **68,** 1730–1748, doi:10.1175/2011JAS3635.1.

——, ——, L. Terray, and B. Joly, 2012: The dynamical link between surface cyclones, upper-tropospheric Rossby wave breaking and the life cycle of the Scandinavian blocking. *Geophys. Res. Lett.,* **39,** L10806, doi:10.1029/2012GL051682.

Pelly, J. L., and B. J. Hoskins, 2003: A new perspective on blocking. *J. Atmos. Sci.,* **60,** 743–755, doi:10.1175/1520-0469(2003)060<0743:ANPOB>2.0.CO;2.

Rivière, G., and I. Orlanski, 2007: Characteristics of the Atlantic storm-track eddy activity and its relation with the North Atlantic Oscillation. *J. Atmos. Sci.,* **64,** 241–266, doi:10.1175/JAS3850.1.

Santos, J. A., J. G. Pinto, and U. Ulbrich, 2009: On the development of strong ridge episodes over the eastern North Atlantic. *Geophys. Res. Lett.,* **36,** L17804, doi:10.1029/2009GL039086.

Scaife, A. A., C. K. Folland, L. V. Alexander, A. Moberg, and J. R. Knight, 2008: European climate extremes and the North Atlantic Oscillation. *J. Climate,* **21,** 72–83, doi:10.1175/2007JCLI1631.1.

Scherrer, S., M. Croci-Maspoli, C. Schwierz, and C. Appenzeller, 2006: Two- dimensional indices of atmospheric blocking and their statistical relationship with winter climate patterns in the Euro-Atlantic region. *Int. J. Climatol.,* **26,** 233–249, doi:10.1002/joc.1250.

Seager, R., Y. Kushnir, J. Nakamura, M. Ting, and N. Naik, 2010: Northern Hemisphere winter snow anomalies: ENSO, NAO and the winter of 2009/10. *Geophys. Res. Lett.,* **37,** L14703, doi:10.1029/2010GL043830.

Shabbar, A., J. Huang, and K. Higuchi, 2001: The relationship between the wintertime north Atlantic oscillation and blocking episodes in the north Atlantic. *Int. J. Climatol.,* **21,** 355–369, doi:10.1002/joc.612.

Shutts, G. J., 1983: The propagation of eddies in diffluent jet streams: Eddy vorticity forcing of 'blocking' flow fields. *Quart. J. Roy. Meteor. Soc.,* **109,** 737–761, doi:10.1002/qj.49710946204.

Sillmann, J., and M. Croci-Maspoli, 2009: Present and future atmospheric blocking and its impact on European mean and extreme climate. *Geophys. Res. Lett.,* **36,** L10702, doi:10.1029/2009GL038259.

——, ——, M. Kallache, and R. W. Katz, 2011: Extreme cold winter temperatures in Europe under the influence of North Atlantic atmospheric blocking. *J. Climate,* **24,** 5899–5913, doi:10.1175/2011JCLI4075.1.

Strong, C., and G. Magnusdottir, 2008: How Rossby wave breaking over the Pacific forces the North Atlantic Oscillation. *Geophys. Res. Lett.,* **35,** L10706, doi:10.1029/2008GL033578.

Sung, M.-K., G.-H. Lim, J.-S. Kug, and S.-I. An, 2011: A linkage between the North Atlantic Oscillation and its downstream development due to the existence of a blocking ridge. *J. Geophys. Res.,* **116,** D11107, doi:10.1029/2010JD015006.

Tibaldi, S., and F. Molteni, 1990: On the operational predictability of blocking. *Tellus,* **42A,** 343–365, doi:10.1034/j.1600-0870.1990.t01-2-00003.x.

Tyrlis, E., and B. J. Hoskins, 2008a: Aspects of a Northern Hemisphere atmospheric blocking climatology. *J. Atmos. Sci.,* **65,** 1638–1652, doi:10.1175/2007JAS2337.1.

——, and ——, 2008b: The morphology of Northern Hemisphere blocking. *J. Atmos. Sci.,* **65,** 1638–1652, doi:10.1175/2007JAS2338.1.

Von Storch, H., and F. W. Zwiers, 2001: *Statistical Analysis in Climate Research.* Cambridge University Press, 455 pp.

Wang, Y. H., and G. Magnusdottir, 2012: The shift of the northern node of the NAO and cyclonic Rossby wave breaking. *J. Climate,* **25,** 7973–7982, doi:10.1175/JCLI-D-11-00596.1.

Wiedenmann, J. M., A. R. Lupo, I. I. Mokhov, and E. Tikhonova, 2002: The climatology of blocking anticyclones for the Northern and Southern Hemispheres: Block intensity as a diagnostic. *J. Climate,* **15,** 3459–3473, doi:10.1175/1520-0442(2002)015<3459:TCOBAF>2.0.CO;2.

Woollings, T., and B. Hoskins, 2008: Simultaneous Atlantic–Pacific blocking and the Northern Annular Mode. *Quart. J. Roy. Meteor. Soc.,* **134,** 1635–1646, doi:10.1002/qj.310.

——, and M. Blackburn, 2012: The North Atlantic jet stream under climate change and its relation to the NAO and EA patterns. *J. Climate,* **25,** 886–902, doi:10.1175/JCLI-D-11-00087.1.

——, B. Hoskins, M. Blackburn, and P. Berrisford, 2008: A new Rossby wave–breaking interpretation of the North Atlantic Oscillation. *J. Atmos. Sci.,* **65,** 609–626, doi:10.1175/2007JAS2347.1.

——, A. Hannachi, and B. Hoskins, 2010a: Variability of the North Atlantic eddy-driven jet stream. *Quart. J. Roy. Meteor. Soc.,* **136,** 856–868, doi:10.1002/qj.625.

——, ——, ——, and A. Turner, 2010b: A regime view of the North Atlantic Oscillation and its response to anthropogenic forcing. *J. Climate,* **23,** 1291–1307, doi:10.1175/2009JCLI3087.1.

Yamazaki, A., and H. Itoh, 2013: Vortex–vortex interactions for the maintenance of blocking. Part I: The selective absorption mechanism and a case study. *J. Atmos. Sci.,* **70,** 725–742, doi:10.1175/JAS-D-11-0295.1.

Yiou, P., and M. Nogaj, 2004: Extreme climatic events and weather regimes over the North Atlantic: When and where? *Geophys. Res. Lett.,* **31,** L07202, doi:10.1029/2003GL019119.

Zhang, X., C. Lu, and Z. Guan, 2012: Weakened cyclones, intensified anticyclones and recent extreme cold winter weather events in Eurasia. *Environ. Res. Lett.,* **7,** 044044, doi:10.1088/1748-9326/7/4/044044.